

EFFECT OF TRANSVERSE ISOTROPY ON BENDING TENSILE
STRENGTH OF BEDDED SANDSTONE



A Thesis Submitted in Partial Fulfillment of the Requirements for the
Degree of Master of Engineering in Civil, Transportation and
Geo-Resources Engineering
Suranaree University of Technology
Academic Year 2022

ผลกระทบของทรานซ์เวอร์สไอโซทรอปีต่อกำลังรับแรงดึงสูงสุดแบบแรงดัด
ของหินทราย



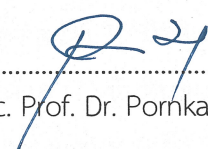
นายสุจินดา จักวาโชติ

วิทยานิพนธ์นี้เป็นส่วนหนึ่งของการศึกษาตามหลักสูตรปริญญาวิศวกรรมศาสตรมหาบัณฑิต
สาขาวิชาวิศวกรรมโยธา ขนส่ง และทรัพยากรธรณี
มหาวิทยาลัยเทคโนโลยีสุรนารี
ปีการศึกษา 2565

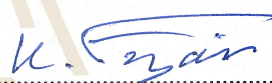
EFFECT OF TRANSVERSE ISOTROPY ON BENDING TENSILE STRENGTH OF
BEDDED SANDSTONE

Suranaree University of Technology has approved this thesis submitted in partial fulfillment of the requirements for a Master's Degree.


Thesis Examining Committee



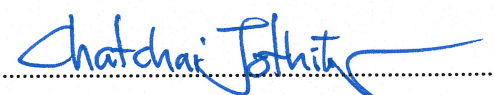
.....
(Assoc. Prof. Dr. Pornkasem Jongpradist)
Chairperson




.....
(Emeritus Prof. Dr. Kittitep Fuenkajorn)
Member (Thesis Advisor)



.....
(Asst. Prof. Dr. Prachya Tepnarong)
Member



.....
(Assoc. Prof. Dr. Chatchai Jothityangkoon)
Vice Rector for Academic Affairs and
Quality Assurance



.....
(Assoc. Prof. Dr. Pornsiri Jongkol)
Dean of Institute of Engineering

สุจินดา จักวาโชติ : ผลกระทบของทรานซ์เวอร์สไอโซทรอปีต่อกำลังรับแรงดึงสูงสุดแบบ
แรงดัดของหินทราย (EFFECT OF TRANSVERSE ISOTROPY ON BENDING TENSILE
STRENGTH OF BEDDED SANDSTONE). อาจารย์ที่ปรึกษา : ศาสตราจารย์ (เกียรติคุณ) ดร.
กิตติเทพ เฟื่องขจร, 75 หน้า.

คำสำคัญ : ระบายชั้นหิน กำลังรับแรงดึง การทดสอบแรงดัดแบบสี่จุด สัมประสิทธิ์ความยืดหยุ่น
อัตราส่วนของปัวซอง

การศึกษานี้มีวัตถุประสงค์เพื่อศึกษาผลของทรานซ์เวอร์สไอโซทรอปีต่อกำลังรับแรงดึงสูงสุด
และคุณสมบัติเชิงยืดหยุ่นของหินทราย หินทรายหมวดหินภูพานถูกคัดเลือกมาทำการทดสอบแรงดัด
แบบสี่จุด ตัวอย่างมีขนาดความกว้างเท่ากับ 30 มิลลิเมตร ความลึก 30 มิลลิเมตร และความยาว 200
มิลลิเมตร การวางแนวระบายชั้นหินแบ่งออกเป็น 2 กรณี ได้แก่ (1) ชั้นหินขนานกับแกนหลัก (2) ชั้น
หินขนานกับทิศทางของแรงกด ระบายชั้นหินจะแปรผันตามตั้งแต่มุม 0 ถึง 90 องศา โดยมีช่วงห่าง
15 องศา ผลการทดสอบระบุว่าผลกระทบของทรานซ์เวอร์สไอโซทรอปีภายใต้แรงดึงเกิดขึ้นโดยมี
กำลังรับแรงดึงแบบแรงดัดมีค่ามากที่สุดเมื่อความเค้นแรงดึงที่เหนี่ยวนำขนานกับระบายชั้นหิน ค่า
เหล่านี้จะค่อยๆ ลดลงจนถึงค่าต่ำสุดเมื่อระบายชั้นหินตั้งฉากกับความเค้นที่เหนี่ยวนำ ค่าสัมประสิทธิ์
ความยืดหยุ่นภายใต้แรงดึงมีค่าต่ำกว่าค่าสัมประสิทธิ์ความยืดหยุ่นภายใต้แรงกด คุณสมบัติเชิง
ยืดหยุ่นของหินทรานซ์เวอร์สไอโซทรอปีจะถูกวิเคราะห์โดยสมการของ Amadei และเปรียบเทียบกับ
ผลการทดสอบ การค้นพบนี้สามารถใช้เพื่อประเมินเสถียรภาพของช่วงหลังคาของการขุดเจาะใต้
ดินภายใต้การวางแนวของระบายชั้นหินที่แตกต่างกันไป

สาขาวิชา เทคโนโลยีธรณี
ปีการศึกษา 2565

ลายมือชื่อนักศึกษา สุจินดา จักวาโชติ
ลายมือชื่ออาจารย์ที่ปรึกษา กิตติเทพ เฟื่องขจร

SUJINDA JAKKAWACHOTE : EFFECT OF TRANSVERSE ISOTROPY ON BENDING
TENSILE STRENGTH OF BEDDED SANDSTONE. THESIS ADVISOR : EMERITUS
PROFESSOR KITTITEP FUENKAJORN, Ph.D., P.E., 75 PP.

KEYWORD : BEDDING PLANE / TENSILE STRENGTH / FOUR-POINT BENDING TEST / ELASTIC
MODULAS / POISSON'S RATIO

The purpose of this study is to determine effect of transverse isotropy on bending tensile strength and elastic properties of bedded sandstone. Phu Phan sandstone is selected for four-point bending test. The prismatic specimens have dimensions of 30 mm in width, 30 mm in depth, and 200 mm in length. Bedding plane orientations are divided into two cases: (1) bedding is parallel to main axis and (2) bedding is parallel to loading direction. Bedding plane orientations β are varied from 0° to 90° with 15° intervals. The results indicate that the transverse isotropic effect under tension occurs where bending tensile strength is largest when induced tensile strengths are parallel to bedding plane orientations. They gradually decrease to the lowest when bedding plane orientations are normal to induced stress. The elastic moduli and Poisson's ratios under tension are lower than those under compression. The elastic properties of transverse isotropic rock are analyzed by Amadei solution and compared with the test results. The findings here can be used to assess the roof span stability of underground excavations under various bedding plane orientations.

School of Geotechnology
Academic Year 2022

Student's Signature สุจินดา จักกาวชอติ
Advisor's Signature ค. ติเทพ

ACKNOWLEDGMENTS

I wish to acknowledge the funding support from Suranaree University of Technology (SUT).

I would like to express thanks to Emeritus Prof. Dr. Kittitep Fuenkajorn, thesis advisor, who gave a critical review. I appreciate his encouragement, suggestions, and comments during the research period. I would like to express thanks to Assoc. Prof. Dr. Pornkasem Jongpradist and Asst. Prof. Dr. Prachya Tepnarong for their valuable suggestions and comments on my research works as thesis committee members. Grateful thanks are given to all staffs of Geomechanics Research Unit, Institute of Engineering who supported my work.

Finally, I most gratefully acknowledge my parents and friends for all their support throughout the period of this study.

Sujinda Jakkawachote

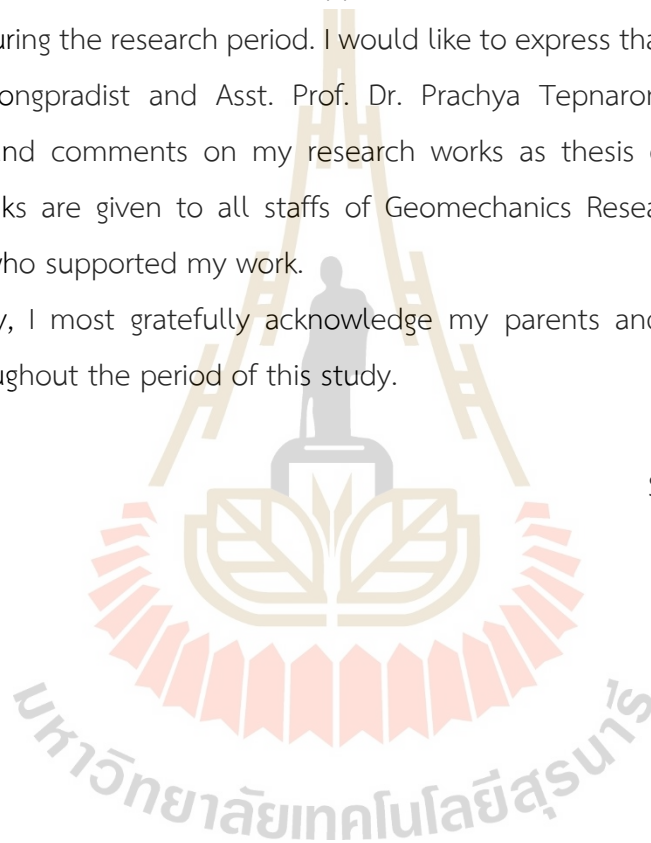


TABLE OF CONTENTS

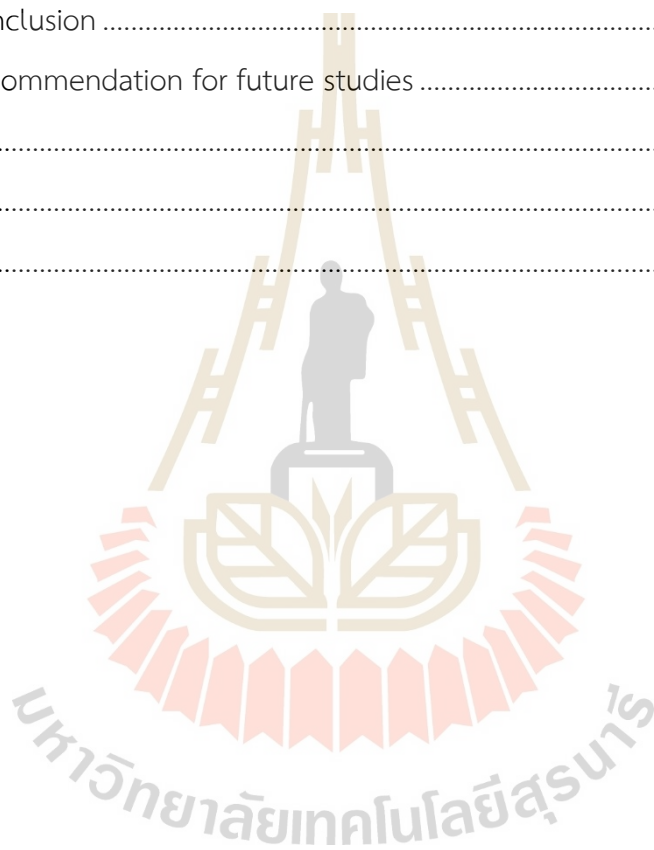
	Page
ABSTRACT (THAI).....	IV
ABSTRACT (ENGLISH).....	V
ACKNOWLEDGEMENT.....	VI
TABLE OF CONTENTS.....	VII
LIST OF TABLES.....	X
LIST OF FIGURES.....	XI
LIST OF ABBREVIATIONS.....	XV
CHAPTER	
1. INTRODUCTION.....	1
1.1 Background and rationale.....	1
1.2 Research objectives.....	1
1.3 Scope and limitations.....	2
1.4 Research methodology.....	2
1.4.1 Literature review.....	2
1.4.2 Sample preparation.....	3
1.4.3 Four-point bending test.....	3
1.4.4 Determination of strength and deformation parameters.....	4
1.4.5 Strength and elastic analysis.....	4
1.4.6 Discussions and conclusions.....	4
1.4.7 Thesis writing.....	4
1.5 Thesis contents.....	4
2. LITERATURE REVIEWS.....	6
2.1 Introduction.....	6
2.2 Classification of anisotropy.....	6

TABLE OF CONTENTS (Continued)

	Page
2.3 Tension test	7
2.3.1 Bending test.....	7
2.3.2 Other tensile tests.....	10
2.4 Effect of transverse isotropy on tensile strength and elastic parameters.....	10
2.4.1 Tensile strength	10
2.4.2 Elastic parameters	15
2.5 Analysis of elastic properties on transverse isotropic effect.....	17
3. SAMPLE PREPARATION.....	22
3.1 Introduction	22
3.2 Phu Phan sandstone occurrence	22
3.3 Sample preparation	23
4. LABORATORY TESTING.....	27
4.1 Introduction	27
4.2 Test method.....	27
4.3 Strain gage installation	29
5. TEST RESULTS	32
5.1 Introduction	32
5.2 Four-point bending test results	32
5.2.1 Bending tensile strength	35
5.2.2 Elastic parameters	37
5.3 Mode of failure	41
6. ANALYSIS OF TEST RESULTS.....	44
6.1 Introduction	44
6.2 Amadei's solution	44
6.3 Degrees of rock anisotropy.....	49

TABLE OF CONTENTS (Continued)

	Page
6.4 Transversely isotropy effect on tensile strength	52
7. DISCUSSIONS AND CONCLUSIONS.....	58
7.1 Discussions	58
7.2 Conclusion	60
7.3 Recommendation for future studies	61
REFERENCES	62
APPENDIX.....	67
BIOGRAPHY	75



LIST OF TABLES

Table	Page
2.1 Classification of degree of anisotropy	21
3.1 Physical properties of four-point bending specimens for both cases	24
3.2 Mineral compositions of Phu Phan sandstone	26
5.1 Tensile strengths and elastic properties from four-point bending test results	36
5.2 Elastic properties under tension and compression from four-point bending test results	38
6.1 Intrinsic elastic parameters for both cases	46
6.2 Degree of anisotropy on tensile strength for Phu Phan sandstone	51
6.3 Degree of anisotropy on compressive and tensile elastic moduli of Phu Phan sandstone	51
6.4 Tensile strengths of Phu Phan sandstone from four-point bending and Brazilian test results	55
6.5 Summary of maximum load under three orientations of bedding plane	57

LIST OF FIGURES

Figure	Page
1.1 Research methodology	3
2.1 Loading diagram	9
2.2 Comparison results of flexural and tensile strength	9
2.3 Relationship between Fracture load and various inclination angles	11
2.4 Impact of joint strength on tensile strength	13
2.5 Tensile strength for ring and Brazilian tests as a function of orientations of foliation plane	14
2.6 Different bedding plane orientations of slate	15
2.7 Elastic moduli of direct tension test under various bedding plane angles	16
2.8 Comparison of elastic bending modulus under three orientations	17
2.9 Apparent Young's moduli and theoretical results from Amadei's prediction under various anisotropy ratios of schist	19
2.10 Polar plots of (a) the apparent elastic moduli and (b) the apparent Poisson's ratios	20
2.11 Anisotropy ratio of various rocks	21
3.1 A Geological map of Khorat Plateau, Northeastern part of Thailand	23
3.2 Sandstone specimens: (a) bedding planes are parallel to main axis, and (b) bedding planes are parallel to main axis	25
3.3 Bedding plane orientation for sandstone specimens varies from 0° to 90° for (a) case 1, and (b) case 2	25
4.1 Four-point bending test arrangement	28
4.2 Schematic diagram for for-point bending test	28

LIST OF FIGURES (Continued)

Figure	Page
4.3 Direction of elastic parameters (E_C and E_T) under compression and tension, where $E_{C,top}$, $E_{T,top}$ are compressive and tensile elastic moduli at top surface, $E_{C,bottom}$, $E_{T,bottom}$ are compressive and tensile elastic moduli at bottom surface, ν_C and ν_T are Poisson's ratio under compression and tension	29
4.4 Schematic diagram for strain gage installation at midsection on (a) top surface and (b) bottom surface	30
4.5 Compressive and tensile stresses distribution at mid-section of specimens	31
5.1 Tensile stress-strain curves under various bedding plane angles for case 1	33
5.2 Compressive stress-strain curves under various bedding plane angles for case 1	34
5.3 Tensile stress-strain curves under various bedding plane angles for case 2	34
5.4 Compressive stress-strain curves under various bedding plane angles for case 2	35
5.5 Bending tensile strengths as a function of bedding plane angle β for both cases	37
5.6 Elastic moduli under tension as a function of bedding plane angle β for both cases	39
5.7 Elastic moduli under compression as a function of bedding plane angle β for both cases	39
5.8 Poisson's ratios under tension as a function of bedding plane angle β for both cases	40
5.9 Poisson's ratios under compression as a function of bedding plane angle β for both cases	41

LIST OF FIGURES (Continued)

Figure	Page
5.10 Post-test specimens for case 1 under bedding plane angles vary from $\beta = 0^\circ$ to 90°	42
5.11 Post-test specimens for case 2 under bedding plane angles vary from $\beta = 0^\circ$ to 90°	43
6.1 Polar plots of apparent elastic moduli under tension and compression for case 1	47
6.2 Polar plots of apparent elastic moduli under tension and compression for case 2	48
6.3 Polar plots of apparent Poisson's ratios under compression and tension for case 1	48
6.4 Polar plots of apparent Poisson's ratios under compression and tension for case 2	49
6.5 Relationship between maximum tensile strength ($\sigma_{T,max}$) and minimum tensile strength ($\sigma_{T,min}$) of Phu Phan sandstone	50
6.6 Relationship between maximum elastic modulus (E_{max}) and minimum elastic modulus (E_{min}) under compression and tension for both cases	52
6.7 Tensile strengths as a function of bedding plane angle compared to those of ① Dou et al. (2019), ② Nova and Zaninetti (1990), ③ Lee and Pietruszczak (2015), ④ Shang et al. (2018), ⑤ Zhong et al. (2020), ⑥ Xiao-jing et al. (2016); ⑦ Suwankeeree (2021), and ⑧ Chen and Hsu (2001)	54
6.8 Tensile strengths of Phu Phan sandstone as a function of bedding plane angle compared between four-point bending and Brazilian tests	55

LIST OF FIGURES (Continued)

Figure	Page
6.9 Comparison of maximum loads under three orientations of bedding plane	56



SYMBOLS AND ABBREVIATIONS

a	=	Compliance component
β	=	The angle between bedding planes with respect to the loading direction
b	=	Beam width
d	=	Beam depth
E_T	=	Tensile elastic modulus
E_C	=	Compressive elastic modulus
E_y	=	Apparent elastic modulus
E'	=	Intrinsic elastic modulus normal to transversely isotropic plane
E	=	Intrinsic elastic modulus parallel to transversely isotropic plane
ϵ_T	=	Tensile strain
ϵ_C	=	Compressive strain
ϵ_{lat}	=	Lateral strain
ϵ_x	=	Strain in x plane
ϵ_y	=	Strain in y plane
ϵ_z	=	Strain in z plane
G'	=	Shear modulus on the plane normal to transversely isotropic plane
G	=	Shear modulus on transversely isotropic plane
L	=	Span length
m	=	Number of misfits each data
n	=	Total number of observations
ν_T	=	Poisson's ratio under tension

SYMBOLS AND ABBREVIATIONS (Continued)

ν_c	=	Poisson's ratio under compression
ν_{yz}	=	Apparent Poisson's ratio on y-z plane
ν_{yx}	=	Apparent Poisson's ratio on y-x plane
ν	=	Intrinsic Poisson's ratio on transversely isotropic plane
ν'	=	Intrinsic Poisson's ratio on the plane normal to transversely isotropic plane
P	=	Applied load
P_{max}	=	Maximum load
s_i	=	Mean misfit
σ_T	=	Tensile stress
σ_C	=	Compressive stress
$X_{j,p}$	=	Predicted data
$X_{j,o}$	=	Observed data

CHAPTER 1

INTRODUCTION

1.1 Background and rationale

Sedimentary and metamorphic rocks normally show well-defined structures in the form of bedding plane, foliation, jointing, or fissuring (Gholami and Rasouli, 2014). These structures are formed by physical and chemical involving transportation, deposition, compaction, and cementation (Hakala et al., 2007). Different orientations of three structures have influenced on rock strength and elastic properties. It also affects the stability of underground excavation or engineering structures. In underground excavation, rock tensile strength dictates the maximum roof span and its stability. Tensile strength is usually obtained by various methods in the laboratory, including Brazilian test, direct tension test, ring test, and bending test. Four-point bending test is however more appropriate for roof span analysis because stress pattern is similar to that of roof span in underground excavation (Plangklang et al., 2017). Several researchers study transversely isotropic effect on tensile strength by various methods (Dou et al. (2019) on three-point bending test, Suwankeeree (2021) on Brazilian test, Nova and zaninetti (1990) on direct tension test, Chen and Hsu (2001) on ring test). They report that the tensile strength of transversely isotropic rocks changes with different bedding plane orientations.

The effect of transverse isotropy on bending tensile strength and elastic parameters on rock has rarely been studied. For underground excavation, these knowledges are needed for the analysis and evaluation of roof span stability under transverse isotropy effect.

1.2 Research objectives

The study is intended to determine bending tensile strength and elastic properties under transversely isotropic effect. Four-point bending test are performed

on Phu Phan sandstone with various bedding plane orientations. The elastic parameters are based on Amadei's solutions. The findings can be used to predict the transverse isotropic behavior on mechanical properties of bedded sandstone. The results for this study also can be used to assess roof span stability of underground excavation with different orientations of bedding plane.

1.3 Scope and Limitations

The scope and limitations of the study include as follows.

- 1) The rock specimens are prepared from Phu Phan sandstone.
- 2) The nominal dimensions of specimens are 30 mm in width, 30 mm in depth, and 200 mm in length.
- 3) The specimens are prepared with different bedding orientations at 0°, 15°, 30°, 45°, 60°, 75° and 90° (The angle is bedding plane with respect to the loading direction).
- 4) The bedding plane orientations are divided into two cases: bedding plane orientations are normal and parallel to main axis.
- 5) The test method is performed in according to ASTM D6272-17 standard practice.
- 6) The applied loading rate at 0.1 MPa/s.

1.4 Research methodology

The research methodology is shown in Figure 1.1 comprises 7 steps; including literature review, samples preparation, four-point bending test, determinations of strength and deformation parameters, strength and elastic analysis, discussions and conclusions, and thesis writing.

1.4.1 Literature review

Literature review is performed to study previous research about classification of anisotropy rock, tension test, effects of transverse isotropy on tensile strength and elastic parameters, and analysis of elastic properties on transversely isotropic effect. The sources of information are obtained from papers journals, and technical reports.

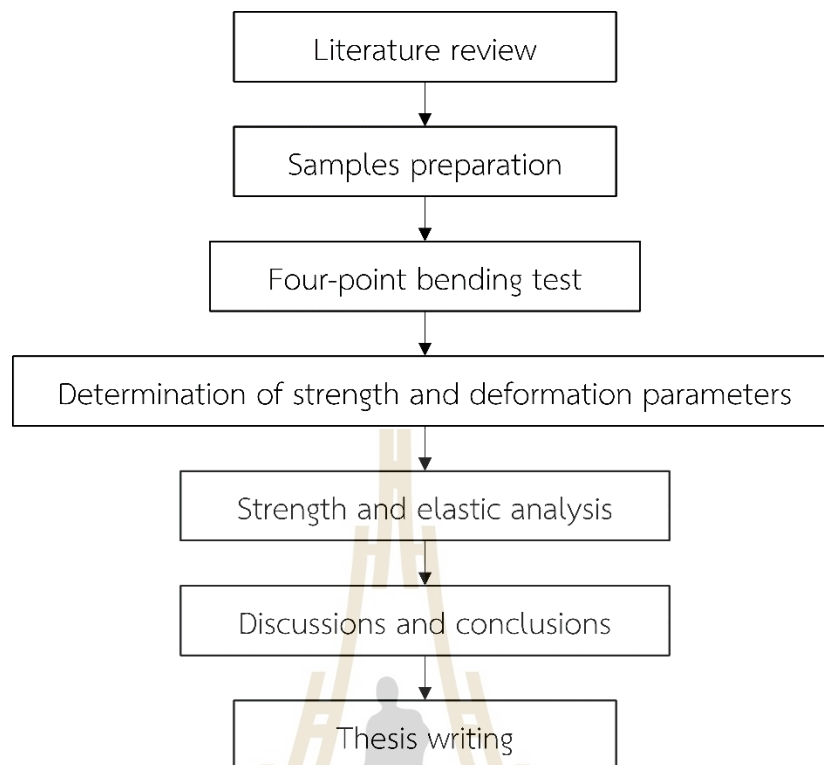


Figure 1.1 Research methodology.

A content of the literature review is summarized in chapter 2 of thesis.

1.4.2 Samples preparation

The rock samples are prepared from Phu Phan sandstones. The sandstone specimens are prepared as prismatic beam with dimensions of 30 mm in width, 30 mm in depth, and 200 mm in length. The bedding plane orientation are varied of 0°, 15°, 30°, 45°, 60°, 75°, and 90°. For both cases, the angle is the bedding plane with respect to loading direction. The bedding plane orientation are divided into two cases: the first case, the beds are parallel the main axis (the bedding plane angles increase according to rotation around x-axis). The second case, the beds are normal the main axis (the bedding plane angles increase according to rotation around z axis). A total of 13 samples are prepared in this study.

1.4.3 Four-point bending test

Four-point bending test is performed in according to ASTM D6272-17 (2020) standard practice. Laboratory tests are carried out in Suranaree University of

Technology. The loading points are placed as one-third of support span. The loading is applied at a rate of 0.1 MPa/s until failure occurs. The strain gages are installed at mid-section on top and bottom of specimen surfaces to measure main and lateral strains. The strain is recorded from data logger (TC-32K), which is connected to the switching box.

1.4.4 Determination of strength and deformation parameters

The measured parameters are plotted in the form of tensile and compressive stress-strain curves. Bending tensile strength, elastic modulus, and Poisson's ratio are present as function of different bedding plane angles. The strength and deformation parameters for both cases are compared under different orientation of bedding plane. Post-test specimens for four-point bending test describe characteristics of mode of failures.

1.4.5 Strength and elastic analysis

The Amadei (1966) solutions are used to assess the apparent elastic moduli and Poisson's ratios under different orientations of bedding planes. The elastic parameters between testing results and analysis are compared. The discrepancy for both data are calculated by mean misfit equation. The tensile strength and elastic parameters are analyzed in the form of degrees of anisotropy.

1.4.6 Discussions and conclusions

Discussions describe the reliability and adequacy of the findings here. The results are compared with sources of information elsewhere. The future research needs are identified in this chapter.

1.4.7 Thesis writing

All research activities and results are documented and complied with in the thesis. This research can be applied to analyze and evaluate roof span stability of underground excavation obtained effect from transversely isotropic rock.

1.5 Thesis content

This thesis is divided into seven chapters. Chapter I introduces about the problems and significance of this study, research objectives, scope and limitations, and research methodology. Chapter II summarizes previous research about classification of

anisotropy rock, bending test, effects of transverse isotropy on tensile strength and elastic parameters, and analysis of elastic properties on transversely isotropic effect. Chapter III describes sample preparation and classification of bedding plane orientation. Chapter IV explains test method about four-point bending test and strain gage installation. Chapter V presents four-point bending results and mode of failures. Chapter VI offers the analysis of test results with Amadei's solution. Chapter VII discusses and concludes the obtained results for this research. Future studies are recommended about further knowledge that should be investigated.



CHAPTER 2

LITERATURE REVIEW

2.1 Introduction

This chapter summarizes the previous research to understand literature review about classification of anisotropy, tension test, Effect of transverse isotropy on tensile strength and elastic parameters, and Analysis of elastic properties on transversely isotropic effect.

2.2 Classification of anisotropy

Hakala et al. (2007) describe the theory of rock anisotropy from Amadei's 1996. Sedimentary and metamorphic rocks demonstrate bedding, stratification, foliation, and jointing. These types of rock have physical, dynamic, thermal, mechanical, and hydraulic properties that vary inherently in anisotropic orientation. Sedimentary rock is characterized as intact laminated, stratified, or bedding, such as sandstones, coal, limestones, shales and siltstones, etc. These anisotropy rocks are formed by physical, and chemical processes involving transportation, deposition, compaction, and cementation.

Gholami and Rasouli (2014) present rock anisotropy classification (Singh et al. 1989). The anisotropy rock is classified according to the cleavage or bedding plane. Rock anisotropy is found mainly in sedimentary and metamorphic rocks. Anisotropy is classified according to the rock's mechanical properties to its highest strength and the lowest at the inclined angle, respectively. The orientation of the cleavage or bedding plane has different angles of inclination, which β is defined as the angle between weak plane and axial load. Types of anisotropy can be classified as follows:

1) Inherent anisotropy

The foliation metamorphic rock is classified in this category. This type of anisotropy is caused by the metamorphism of the rock. The mineral composite and

structures affected by pressure and temperature from tectonic process. It causes the minerals in the rock to be compressed until the mineral changes its structure and forming a parallel orientation to form a foliation. Examples of rocks are schist, slate, gneisses, and phyllite.

2) Induced anisotropy

This type of anisotropy is formed by crystallization or metamorphism of minerals. The minerals are arranged in an orientation plane or layer. The degree of anisotropy at $\beta = 90^\circ$ has a rock strength higher than $\beta = 0^\circ$. It is mainly found in metamorphic, chemical, or crystalline rock.

3) Cleavage or planar anisotropy

This type of anisotropy is formed by crystallization or metamorphism of minerals. This results in the rock being placed in a horizontal plane.

4) U-shaped anisotropy

This type of anisotropy is formed by cleavage set along the orientation plane of mineral. The maximum rock strength is at $\beta = 0^\circ$ and minimum is at $\beta = 90^\circ$. It is mainly found in sedimentary and metamorphic rock.

5) Undulatory anisotropy

This type of anisotropy is formed by rocks with more than one set of cleavage. These rocks are mainly found in Coal and biochemical diatomite.

6) Bedding plan anisotropy

This type of anisotropy is formed by the process of transportation, deposition, compaction, and cementation. These processes cause the sediment to align in the bedding plane or layer. The maximum strength of rock at $\beta = 0^\circ$ and the minimum strength between $\beta = 20^\circ$ and $\beta = 40^\circ$. It is mainly found in sedimentary rocks such as sandstone, siltstone, mudstone, and shale.

2.3 Tension test

2.3.1 Bending test

American society for testing and materials ASTM (D6272-17) specifies method, sample preparation, and calculation for four-point bending test. Testing device consists of loading points and bars of rectangular cross-section or support.

Loading noses are installed on 2 support points. There are total of 2 supports. The distance between loading nose is load span. The load span is both one third and one half of the support, as a shown in Figure 2.1.

The maximum stress occurs between the two loading points. The flexural stress can be calculated from the following equations (ASTM D6272-17, 2020).

For a load span is the a third of the support:

$$S = PL / bd^2 \quad (2.1)$$

For a load span is one half of the support span:

$$S = 3PL / 4bd^2 \quad (2.2)$$

where S is stress in the outer fiber throughout the load span (MPa), P is applied load (N), L is span length (mm.), b is beam width (mm.), and d is beam depth (mm.).

Efe et al. (2019) study the effect of sample size on tensile strength of fine crystalline marble. The experiment is carried out on three-point, four-point bending, and direct tension tests. The four-point bending result is compared with three-point bending and direct tensile tests. The results for all three tests are shown in Figure 2.2. The diagram shows that the average four-point bending strengths under size effect are less than three-point bending strength. The highest four-point bending strength results are found in samples of 32x102x381 mm³ (ASTM). Direct tensile strength is lowest value of 3.19 MPa when compared with bending test. For four-point bending test, Tensile strengths are 3.35, 2.61, and 4.19 times direct tensile strength, respectively.

Hein and Brancheriau (2018) compare the hardness of wood in the three-point and four-point flexural tests. The results indicate that three-point bending tensile strength is 5.2 % higher than that of the four-point bending tensile strength. The different tensile strengths between two tests can be explained from the position of the maximum bending moment and maximum axial fiber stress. For the three-point bending test, the maximum stress is at the bottom of the upper loading point. The maximum stress for four-point bending test is distributed over the area between 2 loading points.

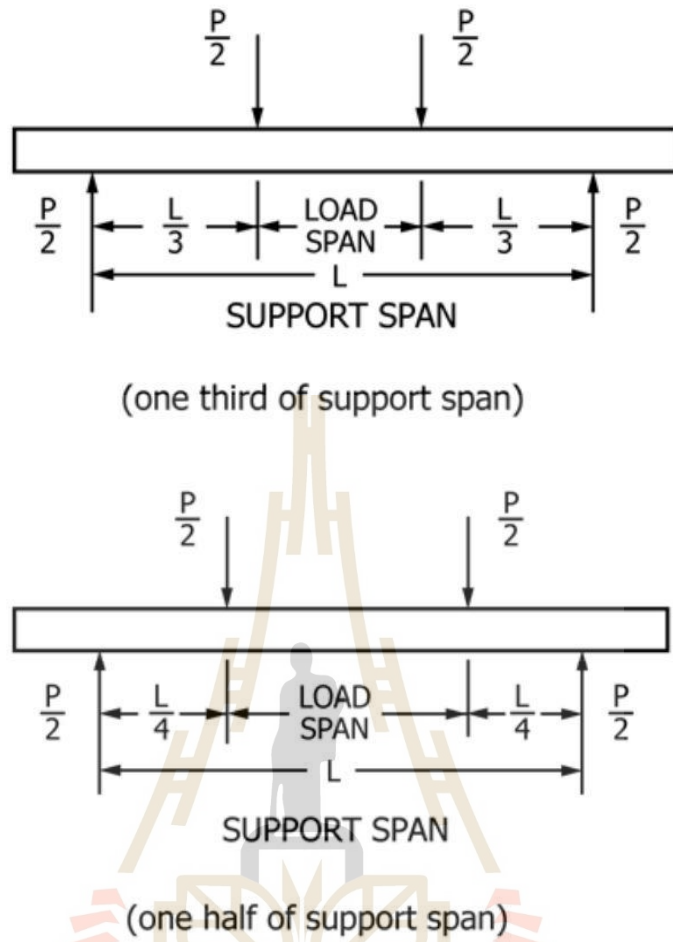


Figure 2.1 Loading diagram (ASTM D6272-17, (2020)).

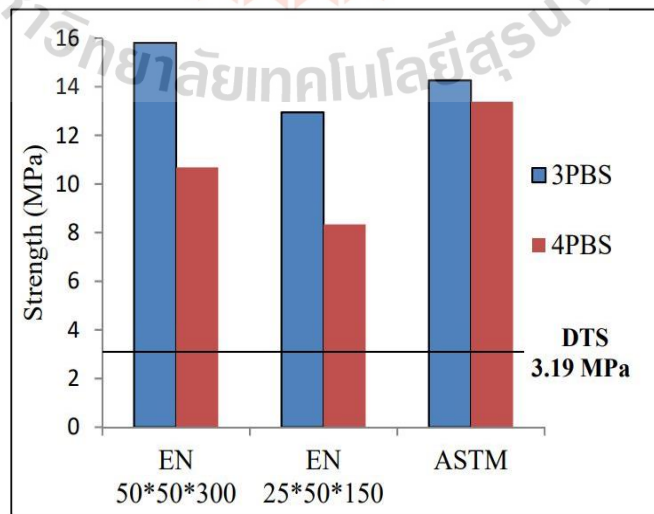


Figure2.2 Comparison results of flexural and tensile strength (Efe et al., 2019).

2.3.2 Other tension tests

Fuenkajorn and Klanphumeesri (2010) conduct direct tension test on intact rock by using compression to tension load converter. Intact rocks include sandstone, marble, and limestone, they are cut to obtain dog-bone-shaped cylinder. The specimens are subjected to uniaxial tension and compression at mid-section. The results for all rock types indicate that elastic parameters under tension are lower than those under compression. This result is similar to Stimpson and Chen (1993), who study the measurement of rock elastic moduli under tension and compression by using combined compression-tension test. They also suggest that the pore space of rock under tension load dilates easier than under compression. The direct tension test is compared with tensile strength of Brazilian and ring tests. The direct tensile strength is lowest when compared with three tension methods. The different tensile strengths occur from the amount and distribution of pore space of rock.

Liao et al. (2019) determine tensile strength of rock under various tension methods, including three-point bending, direct tension, and Brazilian tests. The specimens are prepared with the same rock type. The experiment is performed in laboratory and numerical simulation. Both results are identical trends. The results state that bending tensile strength is the highest among those of three methods. These results tend to be similar to Coviello et al. (2005), who study tensile strength of soft rocks on Brazilian, ring, three-point, and four-point bending tests. They also propose that the tensile strength for each method is dependent on specimen shape but bending test seems to be independent on specimen geometry. Kear and Bunger (2014) suggest that the tensile strengths for various methods differ the value because the highest stresses for these tests distribute across dissimilar rock areas.

2.4 Effect of transverse isotropy on tensile strength and elastic parameters

2.4.1 Tensile strength

Berčáková et al. (2017) study the effect of orientations of foliated metamorphic rock on mechanical properties. Migmatized gneiss is selected for sample preparation. The test method is performed by semi-circular bend tests. There are two

types of orientation: 1) foliated planes are perpendicular to the loading direction and 2) applied loading is parallel to foliated planes. The results conclude that foliated planes perpendicular to the loading direction are higher strength than those parallel foliated planes.

Huang et al. (2020) study influence of the bedding orientation on failure of sandstone. The test is carried out on semi-circular three-point bending test. The sandstone specimens are cut to half of the circle and notch at mid-section on the bottom of the specimen. Rock specimens have different bedding plane orientations. Bedding plane angles (β) are varied from 0° , 30° , 45° , 60° , and 90° . Bedding planes perpendicular to applied loading are observed at $\beta = 90^\circ$. For $\beta = 0^\circ$, bedding planes are parallel to loading direction. Test results for semi-circular three-point bending test as shown in Figure 2.3. The diagram shows the average fracture loads increase from 0.93 to 2.1 kN with increasing bedding plane angles from $\beta = 0^\circ$ to 60° . For $\beta = 90^\circ$, The average fracture load is slightly increasing.

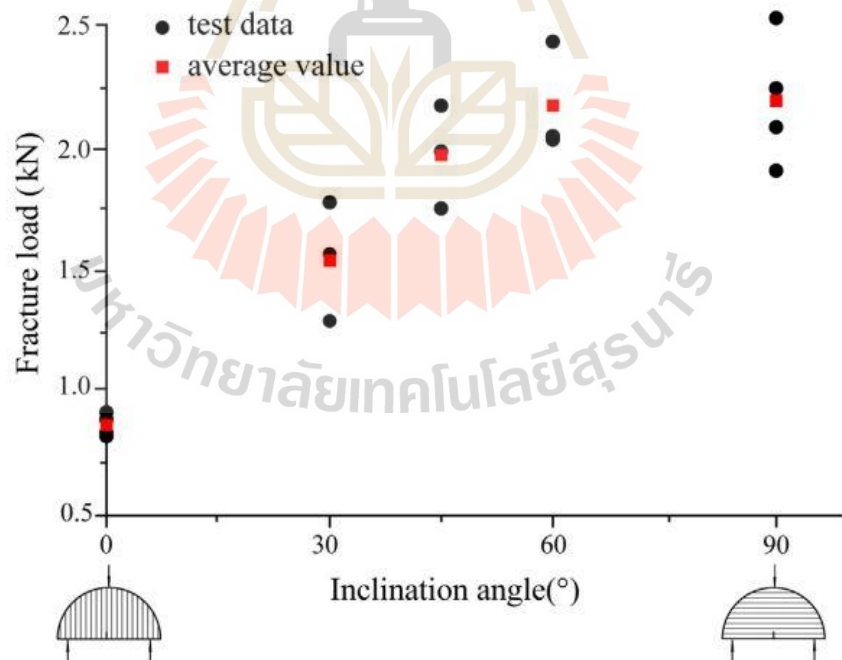


Figure 2.3 Relationship between Fracture load and various inclusion angle (Da hang et al., 2020).

Dou et al. (2019) conduct experiments to study the impact of joint parameters on shale fracture behavior. The test is performed with the three-point bending test. The shale specimens are cut into cubes $80 \times 40 \times 20 \text{ mm}^3$, and notched at 10 mm deep and 2 mm wide. Bedding plane angles are defined of $\beta = 0^\circ, 30^\circ, 60^\circ$ and 90° degrees. The inclined angle is the oblique angle between loading direction and bedding plane orientations. The loading direction is normal to bedding plane orientations at $\beta = 0^\circ$. The applied loading is at a rate of 0.05 mm/min. The three-point bending tensile strengths under different inclined angles are shown in Figure 2.4. The diagram indicates that the three-point bending tensile strength decrease while inclined angles of bedding planes increase.

Liao et al. (1997) study tensile test of transversely isotropic rock. The specimen is subjected to direct tensile test. Argillite is cut to obtain cylindrical block with dimensions of 54.7 mm in diameter and 136 mm in length. The specimen is pulled by a tensile grip machine on its top and bottom. The foliation plane angles are varied of $\beta = 0^\circ, 15^\circ, 30^\circ, 45^\circ, 60^\circ, 75^\circ$, and 90° . The foliation planes at $\beta = 0^\circ$ are perpendicular to applied loading, they are parallel at $\beta = 90^\circ$. Direct tensile strength increases with increasing foliation plane angles. The highest value is found at $\beta = 90^\circ$. The foliation planes at $\beta = 0^\circ$ give to lowest direct tensile strength. This study tends to be identical to results obtained from Shang et al. (2018) on Midgley sandstone, Nova and Zaninetti (1990), and Lee and Pietruszczak (2015) on quartzitic gneiss, who study effect of transverse isotropic on tensile strength by using direct tensile test.

Vervoort et al. (2014) study the behavior of transversely isotropic rock using Brazilian test. Rock samples are divided into 5 types: sandstones, shale, slates, schist, and gneiss. The different bedding plane orientations are inclined from $\beta = 0^\circ$ to 90° with 10° intervals. The bedding plane orientations are perpendicular to applied load at $\beta = 0^\circ$. They are parallel to loading direction at $\beta = 90^\circ$. Test results for all rock specimens state that the maximum fracture loads decrease trend as increasing inclined angles of bedding plane orientations. Young's modulus tends to be similar to fracture load. Several researchers have studied the transversely isotropic effects of Brazilian test. Suwankeeree (2021) study transverse effect on tensile strength of Phu Phan sandstone by using Brazilian test. Zhong et al. (2020) study mechanical properties of

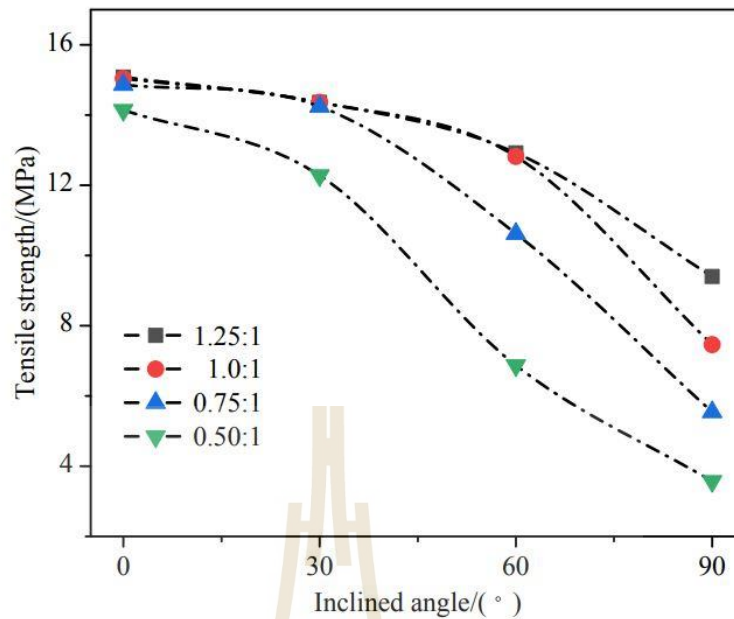


Figure 2.4 Impact of joint strength on tensile strength (Dou et al, 2019).

layered limestone based on Brazilian tension test, Aliabadian et al. (2019) present the fracture initiation in transversely isotropic Hawkesbury sandstone under Brazilian test. Tavallali and Vervoort (2010) study the impact of orientation of bedding on failure strength and fractures sandstone. Khanlari et al. (2014) explain strength of anisotropic foliated rocks under Brazilian tests. Ma et al. (2018) study Brazilian tensile strength of anisotropy rock. Xiao-jing et al. (2016) study influence of bedding orientation on tensile strength of bedded sandstone under Brazilian disc split test. These researchers tend to give identical results.

Chen and Hsu (2001) present effect of different orientations of foliation plane indirect tensile strength. Hualien marble specimen is selected to conduct on Ring and Brazilian tests. Disc specimens for both tests are prepared with identically external diameter of 7.4 cm. The specimens for ring test are drilled at center disc with different internal diameter of 16.4, 12.8, and 4.8 mm. The internal to external diameter ratios, including 0.222, 0.173, and 0.065. The foliation plane varies from 0° (horizontal plane) to 90° (vertical plane). Figure 2.5 shows the tensile strength for both tests in the form of foliation plane angle. The results indicate that the tensile strengths for both tests decrease as foliation plane angle increases. The internal to external diameter ratios of

0.065 give highest tensile strength and decrease trend with increasing ratio. For Brazilian test, their tensile strength is lower than that for ring test.

Pires et al. (2011) study experiments on the flexural strength of slate. The experiment is performed by four-point flexure test. The slate specimens are tested in three different bedding plane orientations, as shown in Figure 2.6. (a) Load is applied perpendicular to the schistosity plane. (b) and (c) applied load is parallel according to bedding planes. The bedding planes for (b) are parallel along length of specimen. For (c), they are parallel with width. The test results state that the four-point flexural strength of orientation (a) is higher than those of orientations (b) and (c). The mean four-point flexural strengths of orientations (a), (b), and (c) are 42.5, 32.3, and 0.49 MPa, respectively. This experiment concluded that bedding plane orientations have a great influence on flexural strength. These results tend to be similar to those obtained by Wu et al. (2017) on mudstone and coal; Li et al. (2019); Kramarov et al. (2020); Heng et al. (2020); Ren et al. (2021) on shale, who study three orientations of bedding plane on three-point bending tensile strength.

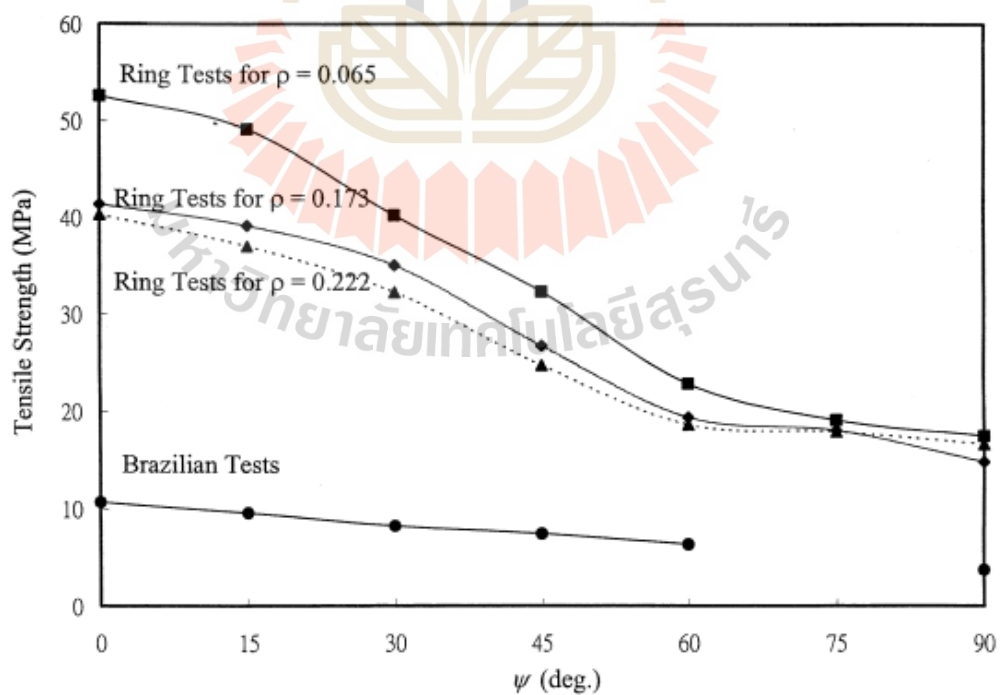


Figure 2.5 Tensile strength for ring and Brazilian tests as a function of orientations of foliation plane (Chen and Hsu, 2001).

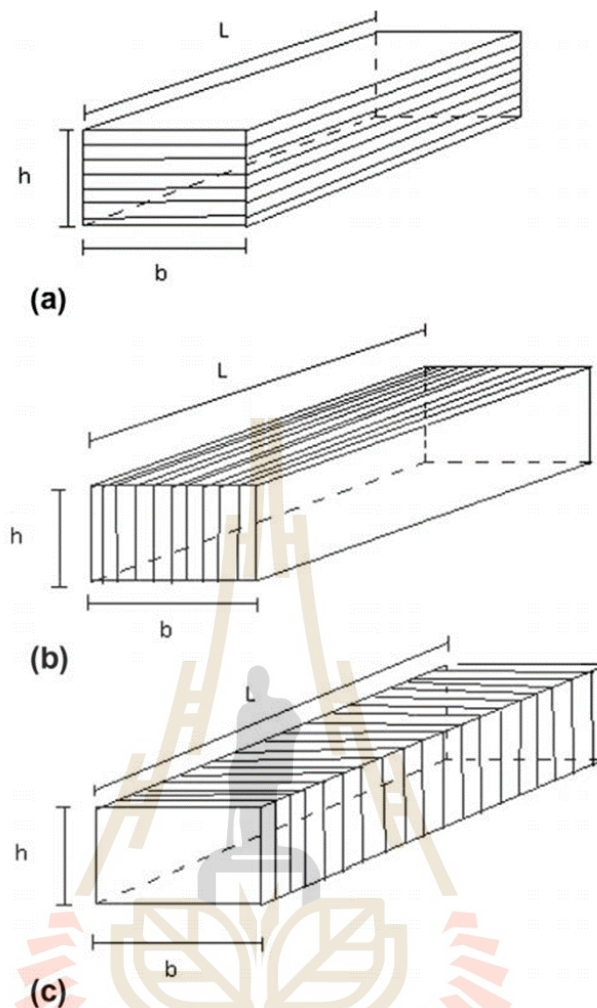


Figure 2.6 Different bedding plane orientations of slate (Pires et al, 2011).

2.4.2 Elastic parameters

Nova and zaninetti (1990) study transverse isotropic behavior of schistose rock. The experiments are performed by direct tensile test. Quartzitic gneiss are prepared as cores of 50 mm in diameter and 150 mm in length. The rock samples have different orientations of schistosity of 0° , 15° , 30° , 45° , 60° , 75° , and 90° (The bedding plane angle is loading direction with respect to the schistosity plane). Figure 2.7 shows that the elastic moduli tend to increase with decreasing of bedding plane angles. The tensile elastic moduli are highest when bedding plane parallel to tensile stress. They are the lowest value as the stress normal to bedding plane orientations.

Sui et al. (2023) study mechanical properties of shale anisotropy by using three-point bending test under three orientations of bedding plane. The bedding planes are divided into 3 types, including arrester, divider, and short transverse orientation. Arrester orientation is bedding plane normal to loading direction. Divider orientation is bedding plane parallel to length of beam specimen. Short transverse orientation is bedding plane parallel to depth of beam specimen. The results show elastic moduli in the form comparing three orientations as show in Figure 2.8. The diagram shows that the divider orientation is largest elastic bending modulus and lowest values on short transverse orientation. For arrester orientation, they give medium elastic bending modulus.

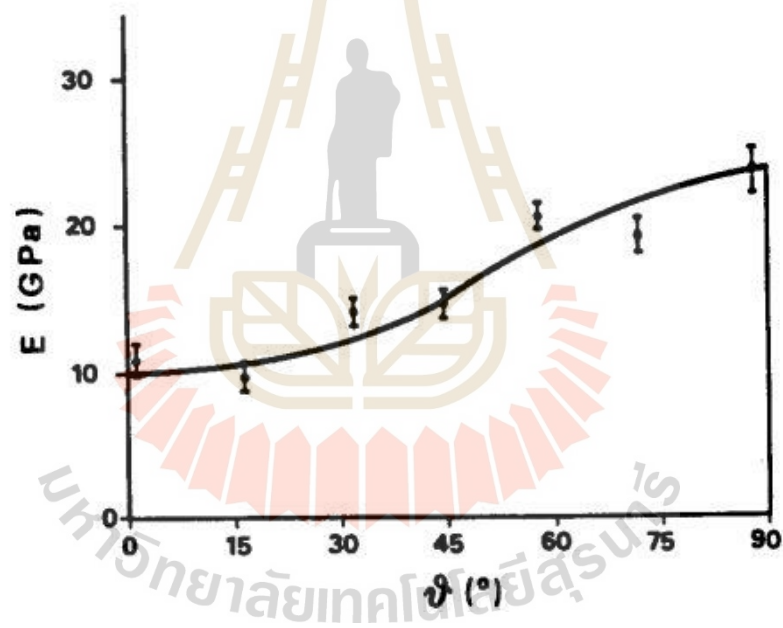


Figure 2.7 Elastic moduli of direct tension test under various bedding plane angles (Nova and Zaninetti, 1990).

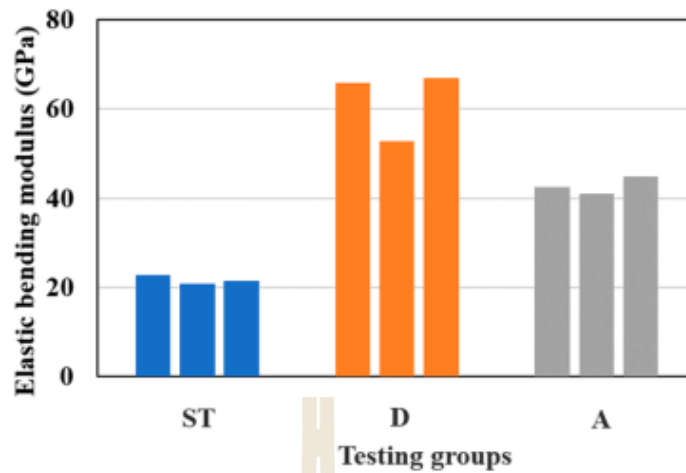


Figure 2.8 Comparison of elastic bending modulus under three orientations (Sui et al., 2023).

2.5 Analysis of elastic properties on transversely isotropic effect

Amadei (1996) proposes theory and prediction of elasticity on anisotropic rock. This theory is carried out with various laboratory tests such as: bending, Brazilian, multiaxial compression, triaxial compression, triaxial compression, and torsion tests. An x, y, and z coordinate system are attached to the specimen. The transverse isotropic planes are parallel to z axis. An angle β is x plane with respect to z plane. The required elastic parameters for analysis are E, E', ν , ν' and G'. The strains for transverse isotropic rock can be obtained from equation as follows;

$$\varepsilon_x = a_{12}\sigma; \quad \varepsilon_y = a_{22}\sigma; \quad \varepsilon_z = a_{23}\sigma \quad (2.3)$$

where a_{12} , a_{22} , and a_{23} are compliance components. These values can be obtained as follows:

$$a_{12} = -\nu'/E'\sin^4\beta - \nu'/E'\cos^4\beta + \sin^2 2\beta/4(1/E+1/E'-1/G') \quad (2.4)$$

$$a_{22} = \cos^4\beta/E' + \sin^4\beta/E + \sin^2 2\beta/4(1/G' - 2\nu'/E') \quad (2.5)$$

$$a_{23} = (\nu'/E')\cos 2\beta - (\nu/E)\sin^2\beta \quad (2.6)$$

where E and E' are the intrinsic Young's moduli on parallel and normal to bedding plane orientation, respectively, ν and ν' are the intrinsic Poisson's ratios characterizing the lateral strain response in the bedding plane parallel and normal to loading direction, G' is the shear modulus in bedding planes normal to the transverse isotropy plane, and G is not dependent.

The compliance component is variable to determine the apparent elastic parameters for transverse isotropic rock, it can be calculated as follows;

$$E_y = 1/a_{22} \quad (2.7)$$

$$\nu_{yx} = a_{23}/a_{22} \quad (2.8)$$

$$\nu_{yz} = a_{23}/a_{22} \quad (2.9)$$

where E_y is apparent Young's modulus in x, y and z coordinate systems, ν_{yz} is Poisson's ratio on y-z plane.

Cho et al. (2012) study anisotropic effect on deformation of rock. Gneiss, shale, schist specimens are conducted on uniaxial compressive test. The deformation analysis is based on the theory of elasticity on anisotropic rock by Amadei (1996). Figure 2.9 shows the test and theoretical data of apparent Young's moduli of schist in the form of anisotropy angle. The results indicate that the highest apparent Young's moduli are observed when applied loading parallel to bedding plane. The applied load normal to bedding plane gives the lowest value. The diagram also shows that the test data tend to be the same as theoretical line, this result agrees well with the theory of Amadei prediction. Several researchers study the effect of transverse isotropy on the elasticity of rock based on theory of Amadei prediction. Yun-si et al. (2012) analyze elastic parameters of slate under various bedding plane orientations on uniaxial compressive and Brazilian tests. Gholami and Rasouli (2014) analyze elastic properties of transversely isotropic slate on triaxial compressive test. These researchers give the same agreement with the theory.

Sukjaroen et al. (2021) determine elastic moduli and Poisson's ratios on transversely isotropic rock by using Amadei's solution. Gypsum specimens under

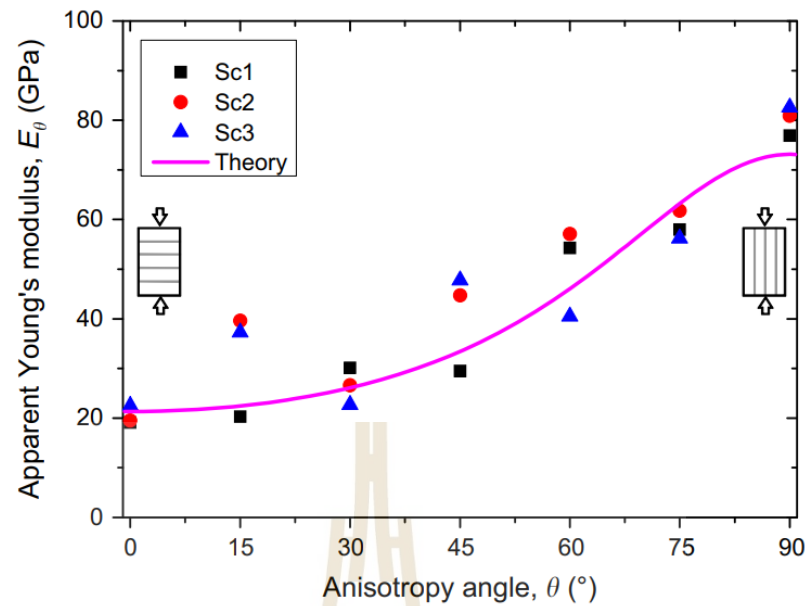


Figure 2.9 Apparent Young's moduli and theoretical results from Amadei's prediction under various anisotropy ratios of schist (Cho et al., 2012).

various bedding plane orientations are conducted on uniaxial and triaxial compressive tests with confining pressure of 0, 3, 7, 12, and 15 MPa. The applied loading is a rate of 0.001, 0.01, 0.1, and 1.0 MPa/s. The results are analyzed in the form of polar plots of the apparent elastic moduli and Poisson's ratios, showing in Figure 2.10. The results reveal that the elastic moduli under different loading rates and bedding plane orientations are similar with increasing the confining pressure. The apparent Poisson's ratios on y-z plane are slight effect on bedding plane orientations. The calculated results are compared with Amadei's prediction. The discrepancy between data and prediction is calculated from mean misfit by Riley et al. (1998), who study mathematical methods for using physics and engineering. The mean misfit can be calculated in equation (2.10). The mean misfit shows that the calculated results provide identical trend of Amadei's prediction. These results tend to be similar to Thongprapha et al. (2022), who study transversely isotropic effect on confining pressure of salt.

$$s_i = 1/m(\sum_i ms_i) \text{ where } s_i = [(1/n) (\sum_{j=1}^n n(X_{j,p}-X_{j,t})^2)]^{1/2} \quad (2.10)$$

where s_i is mean misfit, $X_{j,p}$ and $X_{j,t}$ are the predicted and observed data, n is total number of observations, and m is number of misfit for each data.

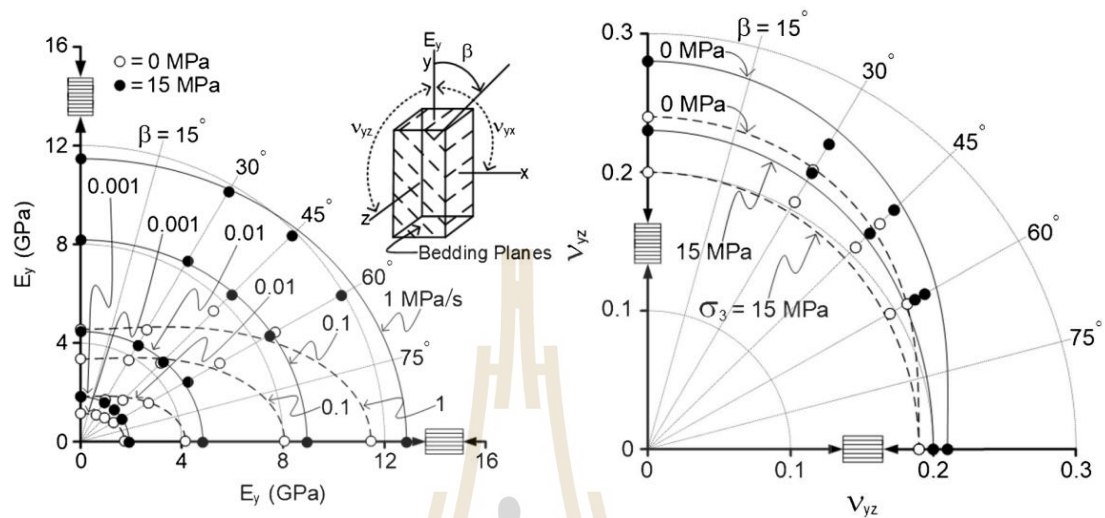


Figure 2.10 Polar plots of (a) the apparent elastic moduli and (b) the apparent Poisson's ratios. (Sukjaroen et al., 2021).

Amadei et al. (1996) present the degree of anisotropy of rock or ratio of maximum to minimum elastic modulus. The maximum and minimum values obtain from bedding plane orientation are normal and parallel to loading direction. The degree of anisotropy varies as 4 range. The quality of anisotropic rock depends on each range of degree of anisotropy. Ramamurthy (1993) classifies the anisotropy ratios as shown in Table 2.1. They divide classification into 5 types include low, medium, high, very high anisotropy, and isotropic. Sedimentary rock normally shows in isotropy and low anisotropic rock. Medium to very high anisotropy can be found in Metamorphic rock.

Ma et al. (2018) study anisotropic degrees on various layered rocks by using Brazilian test. The rock types include shale, sandstone, slate, gneiss, schist, coal, and marl. The anisotropic degree of Brazilian test can be calculated from maximum-to-minimum tensile strength ratios. Figure 2.11 shows the maximum and minimum Brazilian tensile strength of various layered rocks. The diagram shows anisotropic index (AI) are divided into 4 ranges. The anisotropic index includes weak (1-2), medium (2-3),

Table 2.1 Classification of degree of anisotropy

Anisotropy ratio	Class	Rock types
1.0 - 1.1	Isotropic	Sandstone and Shale
1.1 - 2.0	Low anisotropy	
2.0 - 4.0	Medium anisotropy	Slate and Phyllite
4.0 - 6.0	High anisotropy	
More than 6.0	Very high anisotropy	

strong (3-4), and very strong anisotropy (more than 4). The results show that shale and sandstone are normally found weak to strong anisotropy. Slate is weak to very strong anisotropy. Gneiss is weak to medium anisotropy. Schist is medium anisotropy. Coal and Marl are weak anisotropy. Most metamorphic rocks give high anisotropic degrees. For weak to medium anisotropic ratios, they are often found in sedimentary rock.

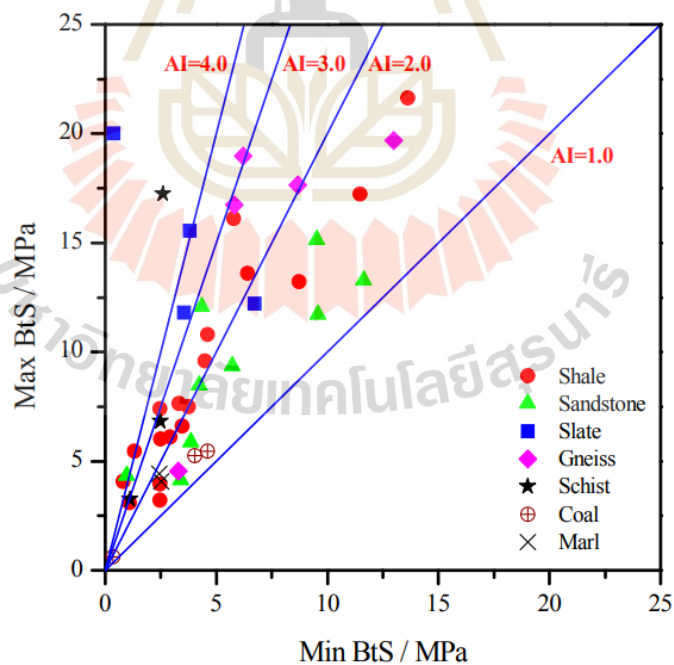


Figure 2.11 Anisotropy ratio of various rocks (Ma et al., 2018).

CHAPTER 3

SAMPLE PREPARATION

3.1 Introduction

This chapter describes the sample preparation for four-point bending test. The Phu Phan sandstone occurrence, sample preparation, and rock properties are indicated in this study. The basic parameters and bedding plane angle of rock specimens are determined.

3.2 Phu Phan sandstone occurrence

Phu Phan sandstone is one of the formations in Khorat group located in Khorat Plateau, Northeastern part of Thailand. Khorat Plateau is an area that affects from the Cretaceous-Triassic tectonic activities. This event uplifts Phu Phan Mountain range, generates continental geosyncline, and creates various secondary structures such as folding, faults, and jointing in regional systems (Veeravinantanakul et al, 2018). Phu Phan sandstone is formed by deposition of continental molasses sediments, these sediments are transported from braided, high-energy and low-sinuosity river (Racey et al., 2009). The eminent Phu Phan formation contains very fine to medium grained size. The bedding planes can be visually observed by gradations of quartz grains and alternating between dark and light brown color. Figure 3.1 shows geological map of Khorat Plateau, Northeastern of Thailand and red box is Phu Phan range. All symbols are shown formation of Khorat groups. Phu Phan formation in geologic map observes as grey color.

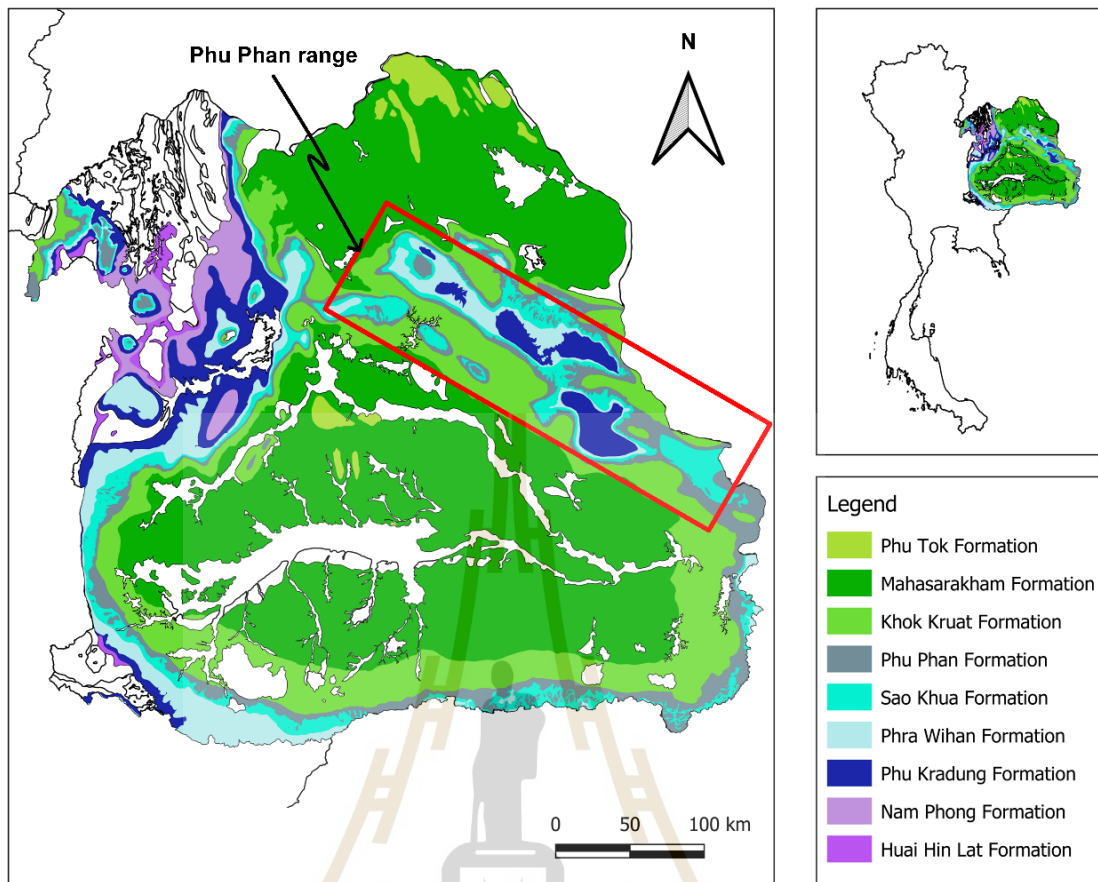


Figure 3.1 A Geological map of Khorat Plateau, Northeastern part of Thailand (Modified from Department of Mineral Resources, 2007).

3.3 Sample preparation

The sandstone specimen has been obtained from Phu Phan formation, Korat Group. Rock specimens are cut to obtain prismatic block with nominal dimensions of $30 \times 30 \times 200 \text{ mm}^3$. Bedding orientations are arranged into two configurations: 1) bedding planes parallel to the main axis (Figure. 3.2a) and 2) beddings normal to the main axis (Figure. 3.2b). For the first case, the beds are rotated around x-axis. The second case shows the beds rotating around z-axis. Normal to the bedding plane makes varied angles (β) with the loading axis from 0° , 15° , 30° , 45° , 60° , 75° to 90° , as a shown in Figure. 3.3. The average density of the specimens is $2.35 \pm 0.04 \text{ g/cc}$. A total of 13 specimens are prepared to perform four-point bending test. Table 3.1 shows dimensions of Phu Phan sandstone specimens for both cases. Specimens for both

cases show identical bedding plane orientation at $\beta = 0^\circ$. The mineral compositions contain 9 minerals, including quartz, oligoclase, albite, chlorite, microcline, anorthite, calcite, kaolinite, and muscovite. The percentages of mineral composition are shown Table 3.2.

Table 3.1 Physical properties of four-point bending specimens for both cases.

Case	Sample No.	Width (mm)	Depth (mm)	Length (mm)	Weight (g)	Density (g/cc)
Case 1	SS-01-0	30.60	30.72	200.38	441.80	2.32
	SS-01-15	31.10	30.38	200.74	454.45	2.33
	SS-01-30	30.90	30.60	200.30	440.47	2.35
	SS-01-45	29.00	30.62	200.02	411.66	2.32
	SS-01-60	28.86	30.82	200.40	416.92	2.34
	SS-01-75	31.00	30.88	200.80	444.95	2.31
	SS-01-90	28.34	30.20	199.60	397.71	2.33
Case 2	SS-02-0	30.60	30.72	200.38	441.80	2.35
	SS-02-15	30.40	30.76	200.20	423.87	2.26
	SS-02-30	31.70	31.42	200.08	453.20	2.27
	SS-02-45	29.60	30.30	199.52	413.23	2.31
	SS-02-60	30.56	30.50	199.60	441.61	2.37
	SS-02-75	30.20	30.40	199.06	435.96	2.39
	SS-02-90	30.70	30.34	200.30	427.57	2.29
Mean \pm SD						2.35 \pm 0.04

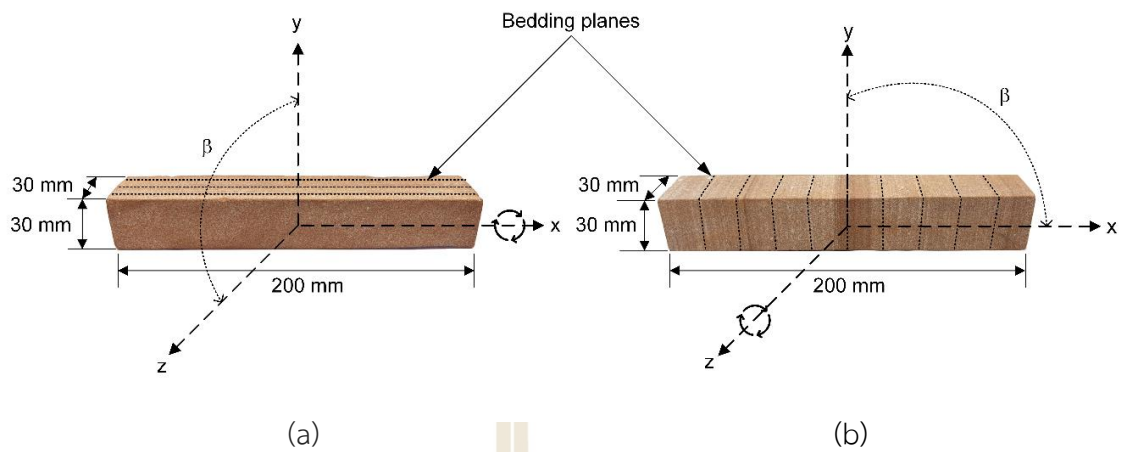


Figure 3.2 Sandstone specimens: (a) bedding planes are parallel to main axis, and (b) bedding planes are parallel to main axis.

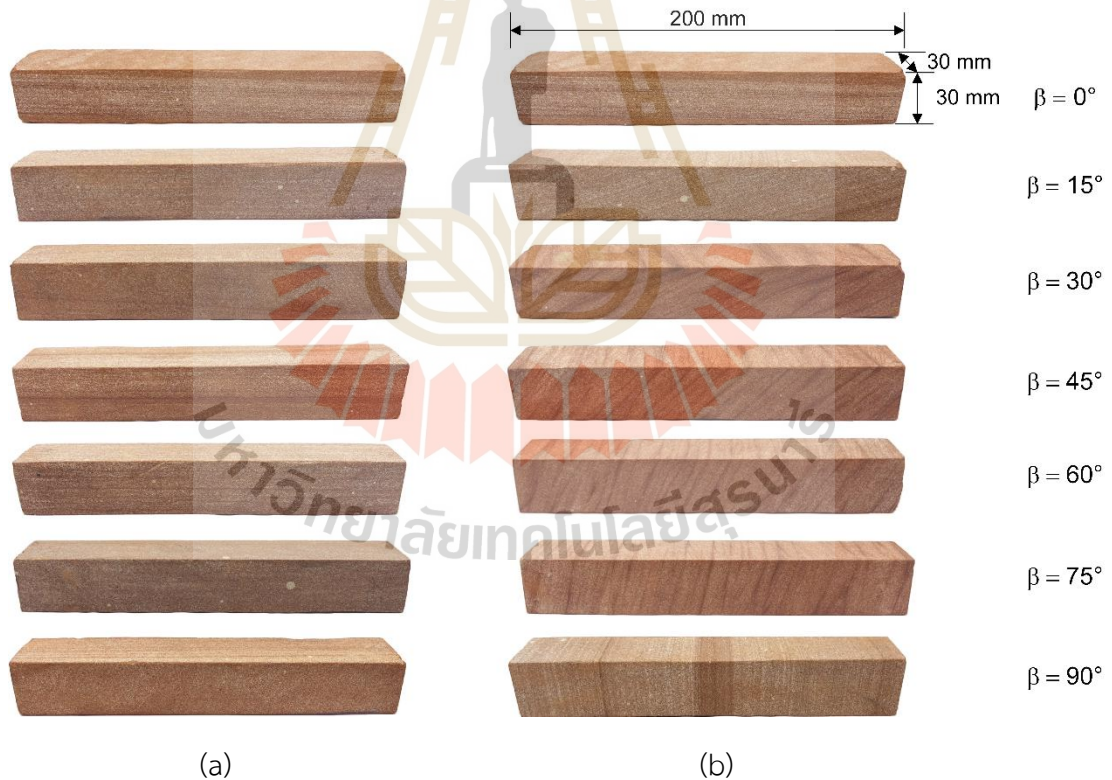
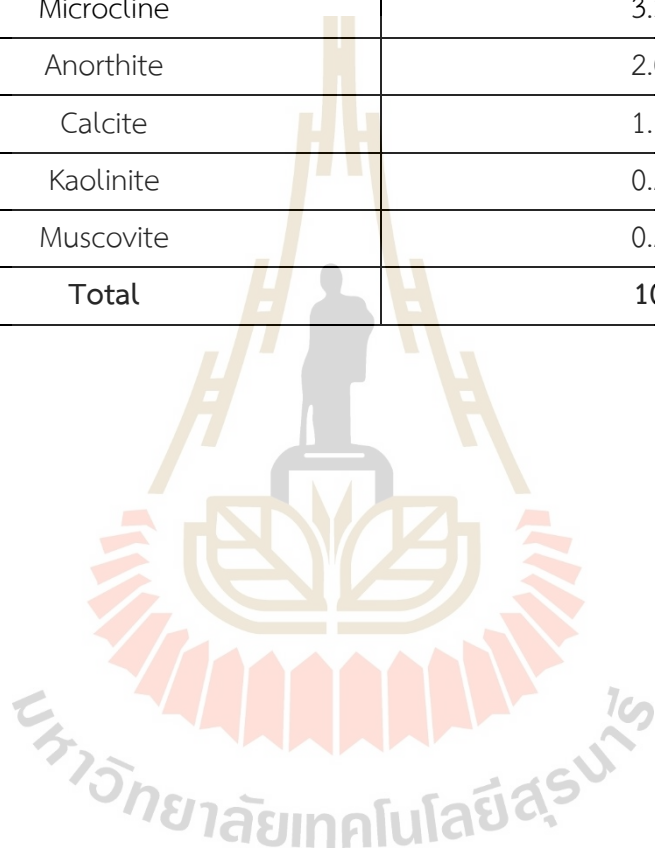


Figure 3.3 Bedding plane orientation for sandstone specimens varies from 0° to 90° for (a) case 1, and (b) case 2.

Table 3.2 Mineral compositions of Phu Phan sandstone.

Mineral composition	Weight (%)
Quartz	67.69
Oligoclase	11.50
Albite	8.26
Chlorite	5.58
Microcline	3.35
Anorthite	2.01
Calcite	1.11
Kaolinite	0.25
Muscovite	0.25
Total	100



CHAPTER 4

LABORATORY TESTING

4.1 Introduction

This chapter describes method and calculation for four-point bending test. The objectives are to determine bending tensile strength and elastic parameters of bedded Phu Phan sandstone under various orientations of bedding plane.

4.2 Test method

The four-point bending test is performed to determine bending tensile strengths and elastic parameters of Phu Phan sandstone specimens under different bedding plane orientations. Test method, equation, and calculation for four-point bending test are carried out in accordance with ASTM D6272-17 standard. Figure 4.1 shows components of apparatus for four-point bending test. They are consisting of hydraulic pump, hand held data logger, switching box, and pressure gage. Specimens are placed on the steel base with 25 mm in diameter. They are placed at the lower steel base with a support span of 180 mm. The upper steel base is arranged with a load span of 60 mm (one-third of support span). All test arrangements for the four-point bending test are shown in Figure 4.2. Loading is applied to the specimens through a spherical bearing at a rate of 0.1 MPa/s until failure occurs. Compressive and tensile stresses at mid-section for four-point bending test specimen can be calculated by ASTM D6272-17, (2020):

$$\sigma_c = +PL / bd^2 \quad (4.1)$$

$$\sigma_t = -PL / bd^2 \quad (4.2)$$

where σ_c is compressive stress, σ_t is tensile stress, P is applied load, L is span length (180 mm), b is specimen width (30 mm), and d is specimen thickness (30 mm).

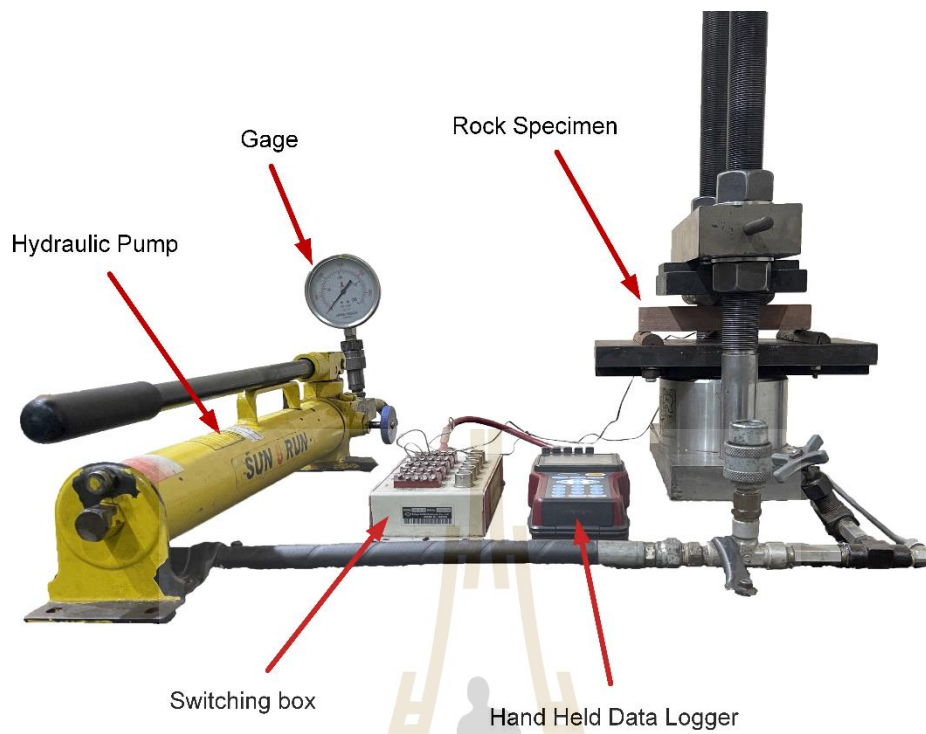


Figure 4.1 Four-point bending test arrangement.

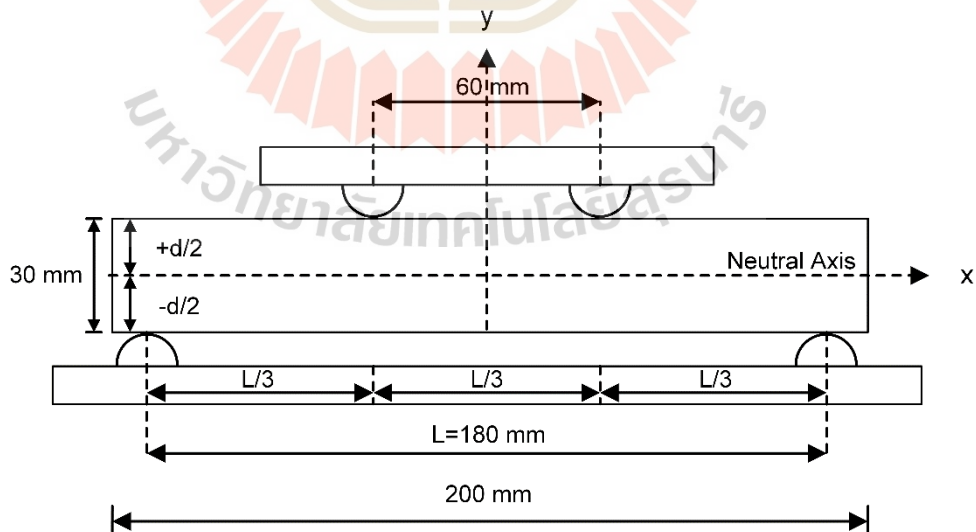


Figure 4.2 Schematic diagram for four-point bending test.

The four-point bending test is a one of indirect tension methods. The specimen is obtained applied load in y axis while the induced stress direction occurs along the length of specimen. The specimen is subjected to non-uniform stresses across its cross-sectional area. The maximum stresses are induced on the specimen surface. The upper surface is subjected to compressive stress and the opposite surface is to tensile stress. The magnitudes of the induced stresses are identical for both sides. The upper surface is under contraction when a compressive stress is applied to specimen. They are extended at opposite side under tension. Poisson's ratio under compression (ν_c) and tension (ν_T) can be calculated from strain gage measurements.

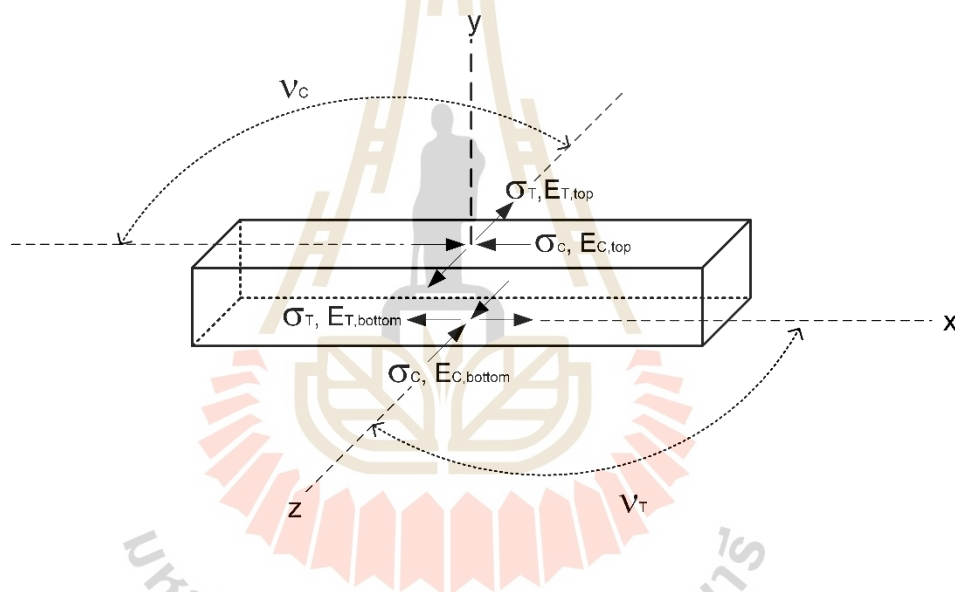


Figure 4.3 Direction of elastic parameters (E_C and E_T) under compression and tension, where $E_{C,top}$, $E_{T,top}$ are compressive and tensile elastic moduli at top surface, $E_{C,bottom}$, $E_{T,bottom}$ are compressive and tensile elastic moduli at bottom surface, ν_c and ν_T are Poisson's ratio under compression and tension.

4.3 Strain gage installation

Strain gages are installed at mid-section on top and bottom of the specimen surfaces, as shown in Figures 4.4(a) and 4.4(b). They are parallel and perpendicular

to the main axis to measure compressive and tensile strains. The gage length is 10 mm, gage resistance is $120 \pm 0.5 \Omega$, and gage factor is $2.12 \pm 1 \%$. Compressive and tensile stresses are induced at top and bottom of the specimens, as shown in Figure 4.5. The strains are recorded with a data logger (TC-32K) connected to a switching box. The obtained strains are used to calculate elastic parameters; elastic modulus and Poisson's ratio.

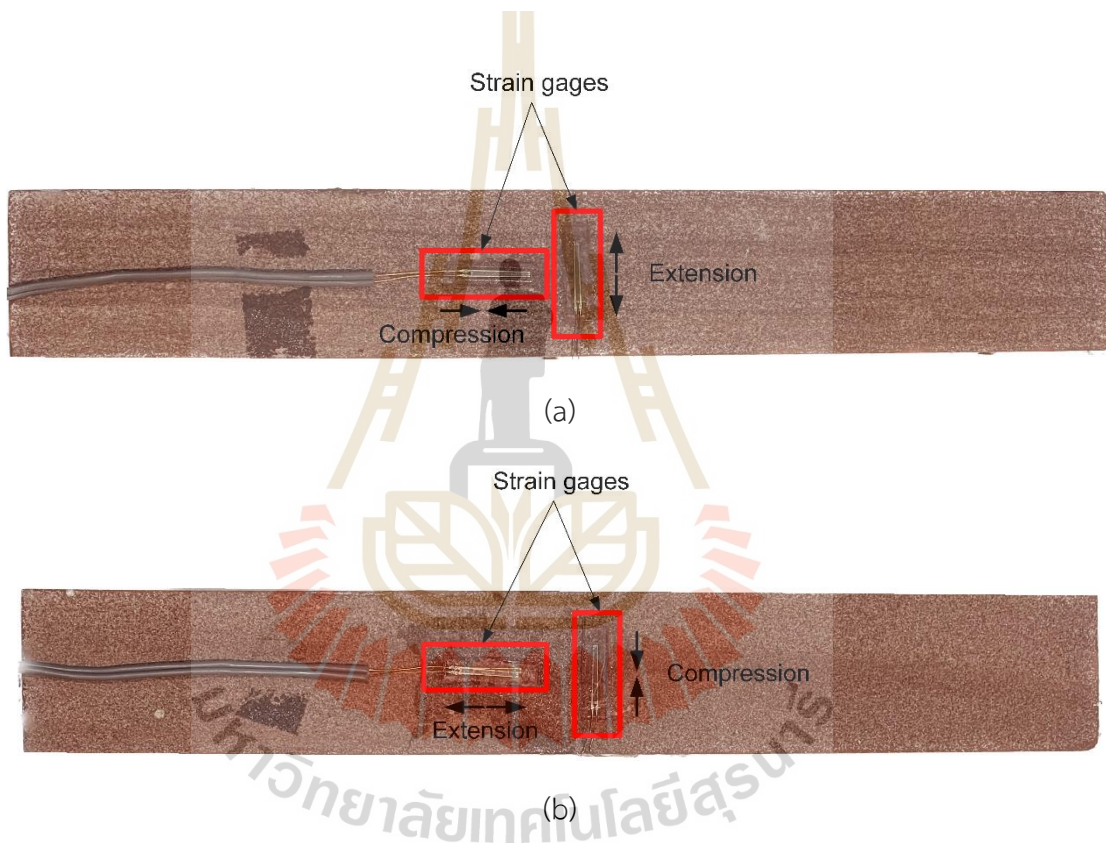


Figure 4.4 Schematic diagram for strain gage installation at midsection on (a) top surface and (b) bottom surface.

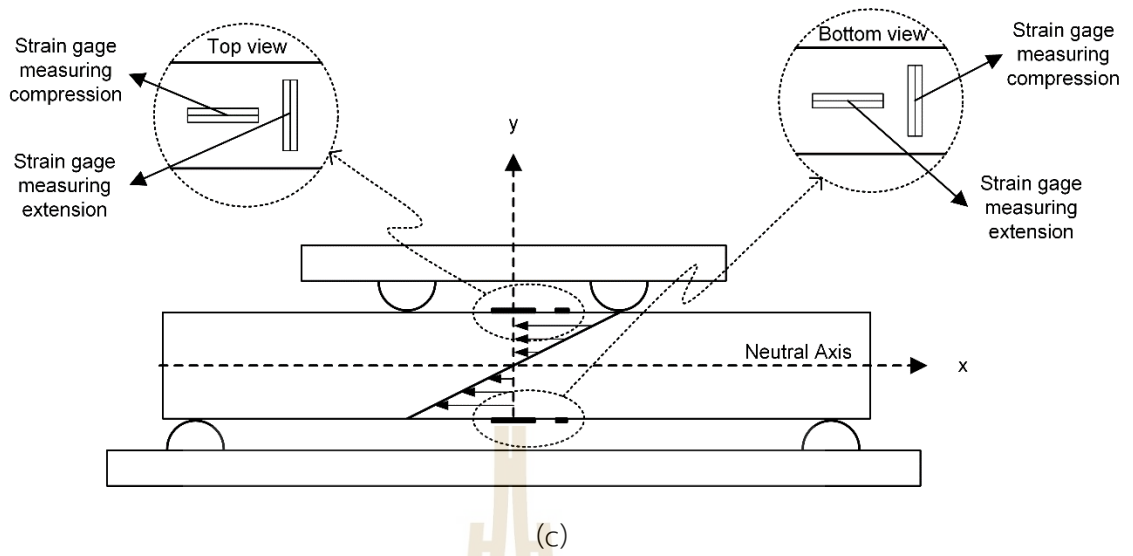


Figure 4.5 Compressive and tensile stresses distribution at mid-section of specimens.

CHAPTER 5

TEST RESULTS

5.1 Introduction

This chapter describes the test results and mode of failure obtained from four-point bending test. The obtained data from testing are used to determine tensile strength and elastic parameters. The test results are shown in the forms of stress-strain curves, tensile strength, and deformation moduli as a function of bedding plane angle. The results in this study are analyzed to identify transversely isotropic behavior and design roof span of underground excavation.

5.2 Four-point bending test results

Figure 5.1 shows tensile stress-strain curves with different bedding plane orientations for case 1, where ϵ_t is tensile strain (negative) and ϵ_{lat} is lateral strain under contraction (positive) on the bottom of specimen surface. The diagram shows that slopes of stress-strain curves are steepest when bedding plane orientations are normal to loading direction at $\beta = 0^\circ$. The lowest slopes are observed for bedding planes parallel to main axis at $\beta = 90^\circ$. For bedding plane orientations at $0^\circ < \beta < 90^\circ$, the curves gradually decrease from 15° to 75° with respect to the rotation around main axis. The curves are terminated at tensile failure corresponding to the specimen's tensile strength. Each curve tends to show nonlinear behavior.

Figure 5.2 shows compressive stress-strain curves with different bedding plane orientations for case 1, where ϵ_c is compressive strain (positive) and ϵ_{lat} is lateral strain under extension (negative) on the top of specimen surface. The compressive stress-strain curves for each bedding plane angle are similar to the results in Figure 5.1. The curves in this diagram show nonlinear behavior. The compressive stress-strain curves are steeper than those under tension. The failure stresses of rock are not found under compression as the magnitude of tensile strength is much smaller than that of the compressive strength.

Figure 5.3 shows tensile stress-strain curves with different bedding plane orientations for case 2. The stress-strain curves are steepest at $\beta = 0^\circ$ (bedding planes are normal to loading direction) and gradually decrease when bedding plane orientations are rotated around z axis until at $\beta = 90^\circ$ (bedding planes are parallel to loading direction). The tensile stress-strain curves are not linear. The failure points for this case are lower than that for case 1.

Compressive stress-strain curves with different bedding plane orientations for case 2 are shown in Figure 5.4. The curves for all bedding plane angles are steep, showing nonlinear behavior.

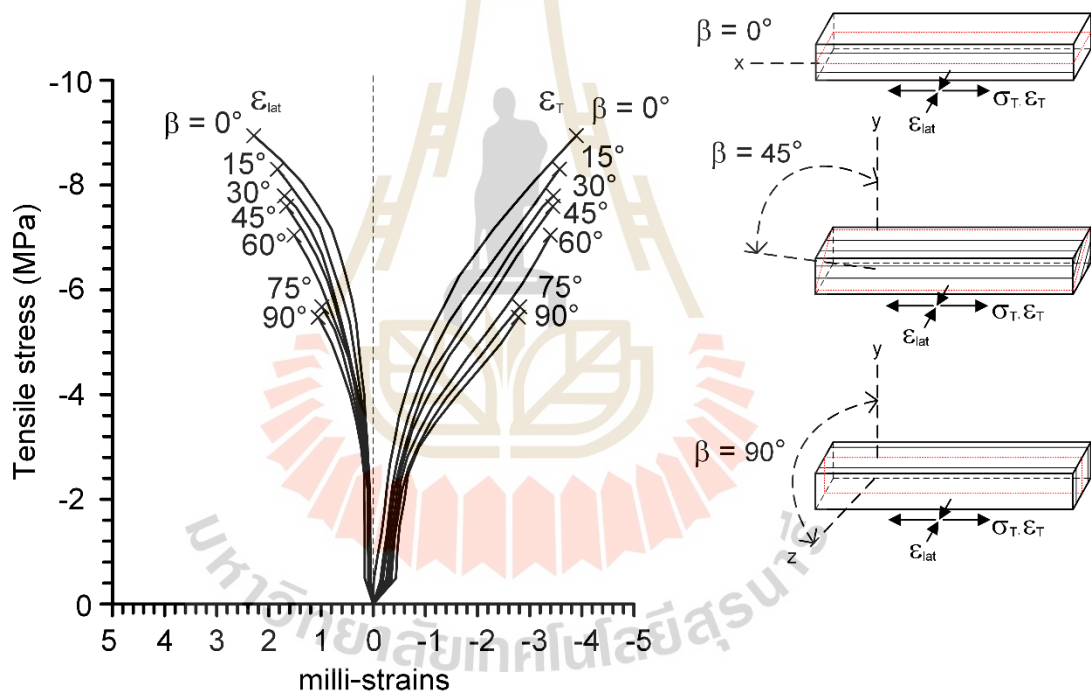


Figure 5.1 Tensile stress-strain curves under various bedding plane angles for case 1.

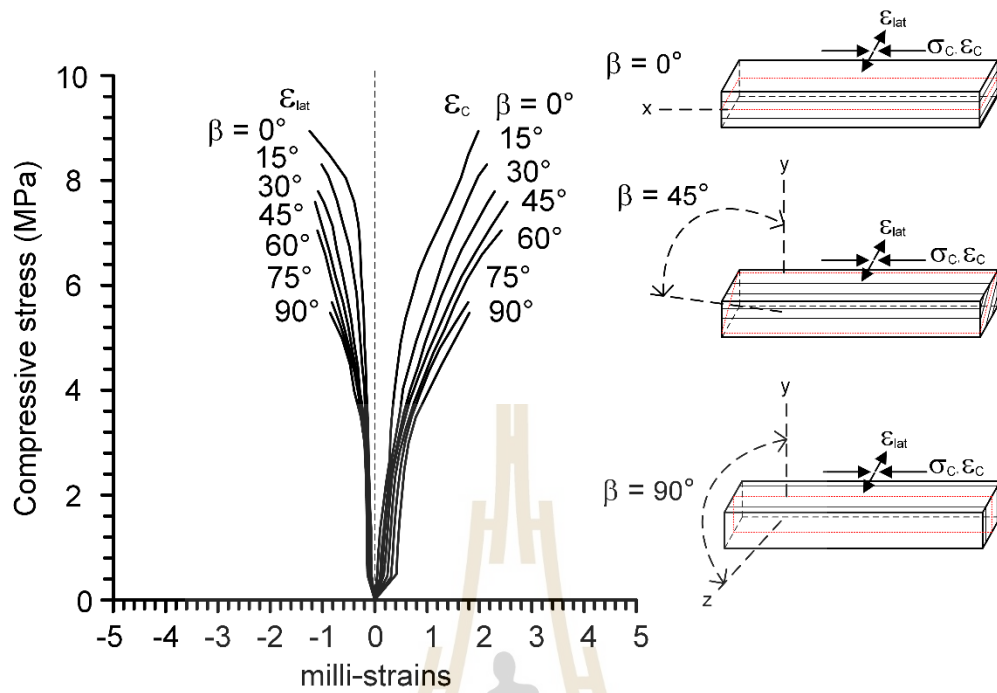


Figure 5.2 Compressive stress-strain curves under various bedding plane angles for case 1.

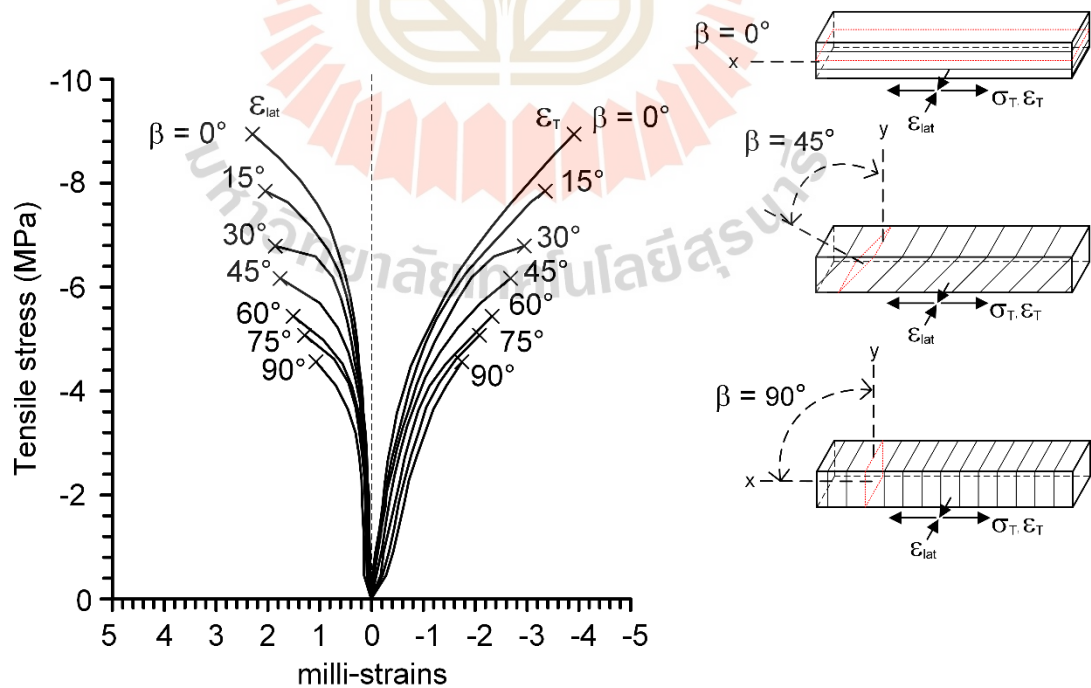


Figure 5.3 Tensile stress-strain curves under various bedding plane angles for case 2.

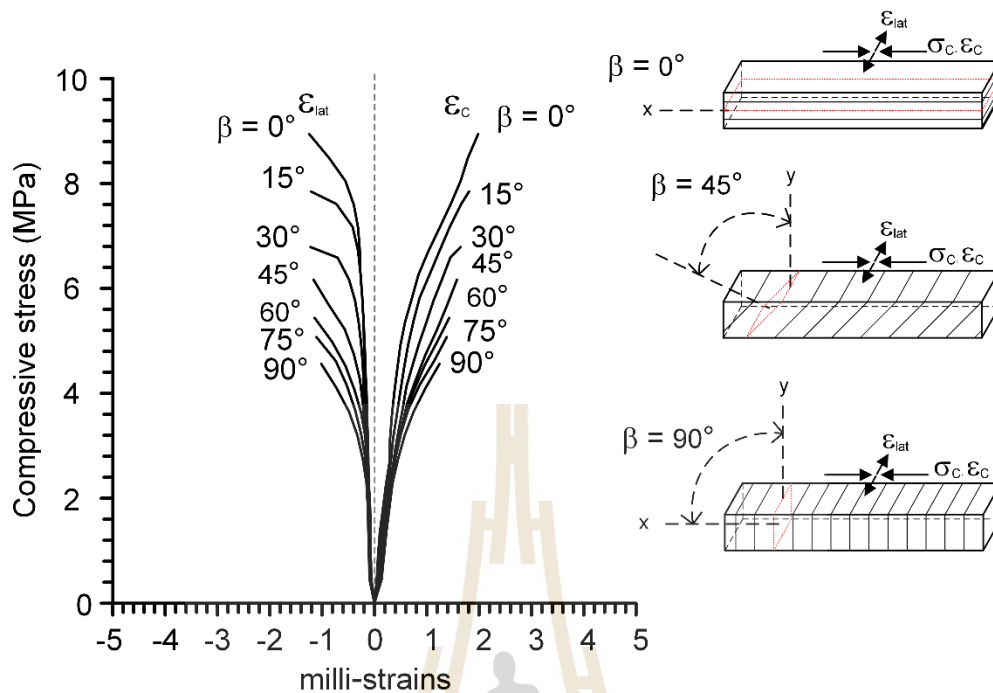


Figure 5.4 Compressive stress-strain curves under various bedding plane angles for case 2.

5.2.1 Bending tensile strength

Bending tensile strength results for both cases are shown in Table 5.1. Figure 5.5. presents the bending tensile strength as a function of bedding plane angles for both cases. The results indicate that the maximum bending tensile strength is found at $\beta = 0^\circ$ (induced tensile stress parallel to bedding plane). At this angle, both cases show identical results. The bedding plane orientations increase from 0° to 90° with 15° intervals and bending tensile strengths for both cases continuously decrease as bedding plane angles β increases. The minimum bending tensile strengths for both cases are found at $\beta = 90^\circ$. For all the bedding plane orientations, bending tensile strength from case 1 (induced tensile stress parallel to bedding plane strike) tends to give higher tensile strength than that from case 2 (induced tensile stress normal to bedding plane).

Table 5.1 Tensile strengths and elastic properties from four-point bending test results.

Case	Sample no.	β (degrees)	$\sigma_{T,f}$ (MPa)
Case 1	SS-01-0	0	8.93
	SS-01-15	15	8.31
	SS-01-30	30	7.80
	SS-01-45	45	7.58
	SS-01-60	60	7.05
	SS-01-75	75	6.10
	SS-01-90	90	5.48
Case 2	SS-02-0	0	8.93
	SS-02-15	15	7.84
	SS-02-30	30	6.80
	SS-02-45	45	6.17
	SS-02-60	60	5.44
	SS-02-75	75	5.08
	SS-02-90	90	4.56

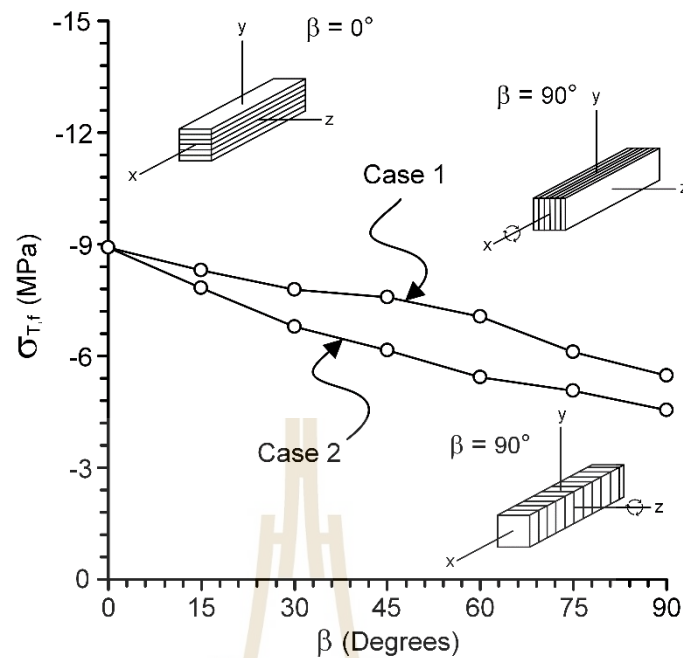


Figure 5.5 Bending tensile strengths as a function of bedding plane angle β for both cases.

5.2.2 Elastic parameters

The results obtained from stress-strain curves are used to determine elastic moduli and Poisson's ratios of the specimens. Table 5.2 gives elastic parameters under tension and compression. Elastic moduli can be obtained from the tangent at a linear portion of stress-strain curve (about 40-50% of failure stress). The tensile elastic moduli for both cases are shown in Figure 5.6. The results show that the tensile elastic moduli for case 1 are largest at $\beta = 90^\circ$ (bedding plane strike parallel to induced stress) and gradually decrease to lowest values at $\beta = 0^\circ$ (bedding plane parallel to induced stress). For case 2, tensile elastic moduli are greatest when bedding plane orientations are parallel to induced tensile strength. They give smallest value where induced stress normal to bedding plane at $\beta = 90^\circ$. This diagram also reveals that elastic moduli under tension for case 1 are greater than those for case 2.

Figure 5.7 shows compressive elastic moduli as a function of bedding plane angles for both cases. The results for both cases tend to give identical result under tension. For both cases, compressive elastic moduli are higher than those under tension.

Table 5.2 Elastic properties under tension and compression from four-point bending test results.

Case	Sample no.	β (degree)	Elastic modulus under tension (GPa)	Elastic modulus under compression (GPa)	Poisson's ratio under tension	Poisson's ratio under compression
Case 1	SS-01-0	0	7.11	10.69	0.08	0.23
	SS-01-15	15	7.84	11.23	0.08	0.23
	SS-01-30	30	7.92	12.04	0.08	0.22
	SS-01-45	45	8.14	12.47	0.07	0.21
	SS-01-60	60	8.25	12.88	0.07	0.21
	SS-01-75	75	8.30	13.11	0.07	0.20
	SS-01-90	90	8.49	13.30	0.07	0.20
Case 2	SS-02-0	0	7.11	10.69	0.08	0.23
	SS-02-15	15	6.57	10.24	0.10	0.24
	SS-02-30	30	6.26	9.81	0.10	0.24
	SS-02-45	45	5.53	9.58	0.11	0.25
	SS-02-60	60	4.85	9.49	0.11	0.25
	SS-02-75	75	4.38	9.33	0.12	0.25
	SS-02-90	90	4.15	9.17	0.12	0.26

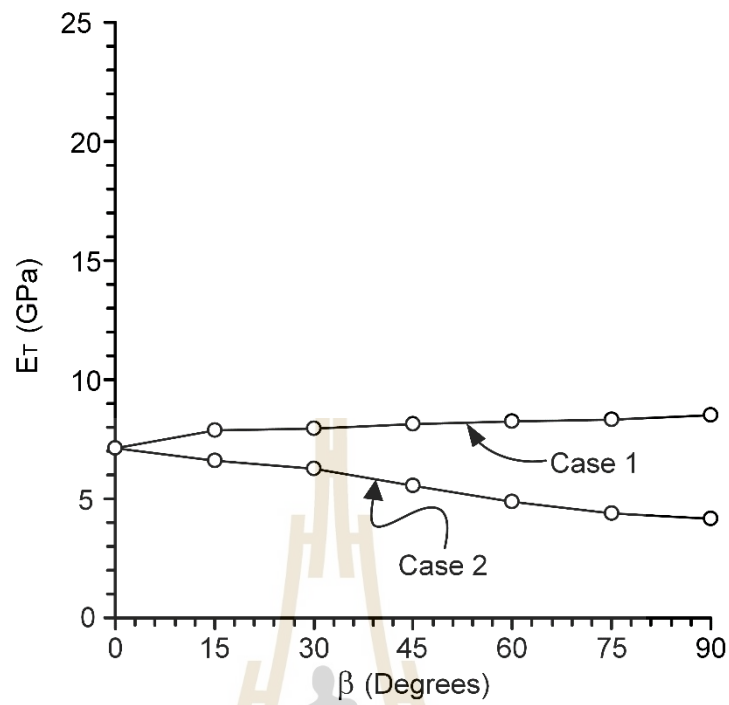


Figure 5.6 Elastic moduli under tension as a function of bedding plane angle β for both cases.

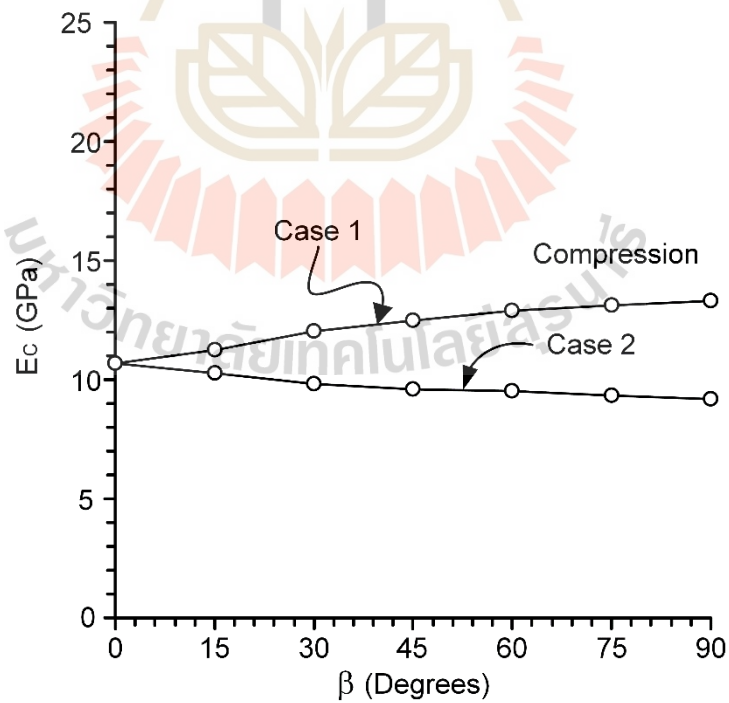


Figure 5.7 Elastic moduli under compression as a function of bedding plane angle β for both cases.

Figure 5.8 shows Poisson's ratio under tension for both cases. Poisson's ratios are in the form of bedding plane angles. The results state that Poisson's ratios under tension for case 2 consistently increase as the bedding plane orientations are rotated toward loading direction around z axis and they are largest at $\beta = 90^\circ$. For case 1, Poisson's ratio tends to contrary results for case 2, the value slightly decreases from $\beta = 0^\circ$ to 90° with rotating around x axis of bedding plane angles. Poisson's ratio under tension for case 1 tends to be relatively low.

Poisson's ratios under compression for both cases are shown in Figure 5.9. The diagram indicates that the Poisson's ratios for case 2 show increasing trend with increasing bedding plane angles from $\beta = 0^\circ$ to 90° . For case 1, the values show a decreasing trend. Poisson's ratios under compression are higher than those under tension.

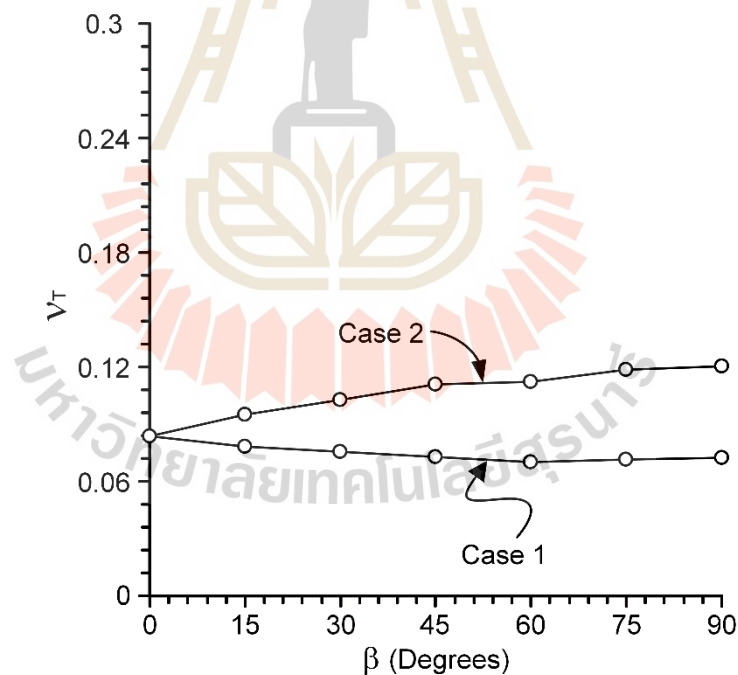


Figure 5.8 Poisson's ratios under tension as a function of bedding plane angle β for both cases.

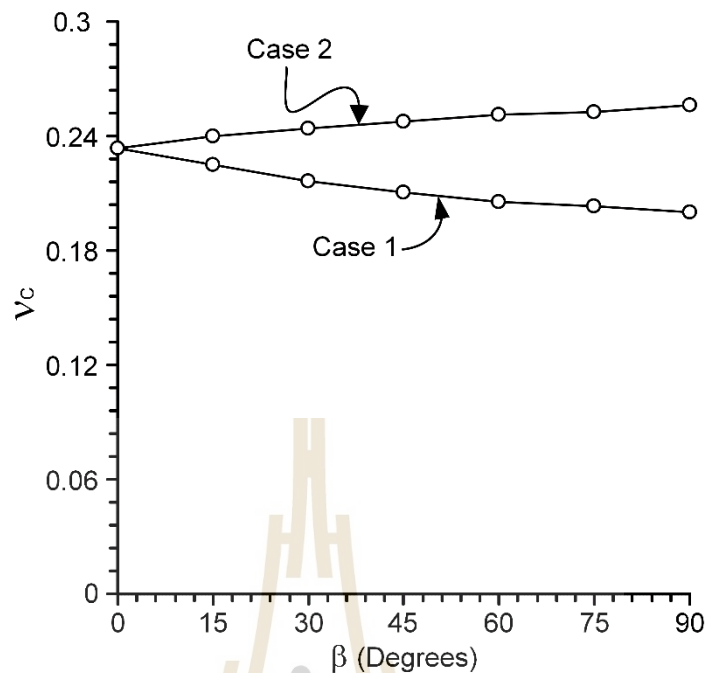


Figure 5.9 Poisson's ratios under compression as a function of bedding plane angle β for both cases.

5.3 Mode of failure

The specimens are bent by four-loading points and fail under tensile stress before they fail under compressive stress. The maximum tensile strength occurs at mid-section on the bottom of specimen surfaces. Figure 5.10 shows post-test specimens for case 1. All specimens for this case show tensile failure induced at the mid-section. The fracture is perpendicular to the bedding plane for specimens with $\beta = 0^\circ$ to 90° .

Figure 5.11 shows mode of failures of four-point bending test for case 2. For this case, the specimens show tensile failure and crack at mid-section through the bedding plane in the range of $0^\circ \leq \beta \leq 30^\circ$. For bedding plane angle at $\beta = 45^\circ$ to 90° , specimens show fracture along bedding planes. They indicate that bedding plane angles that close to the loading direction significantly affect the failure mode of Phu Phan sandstone.

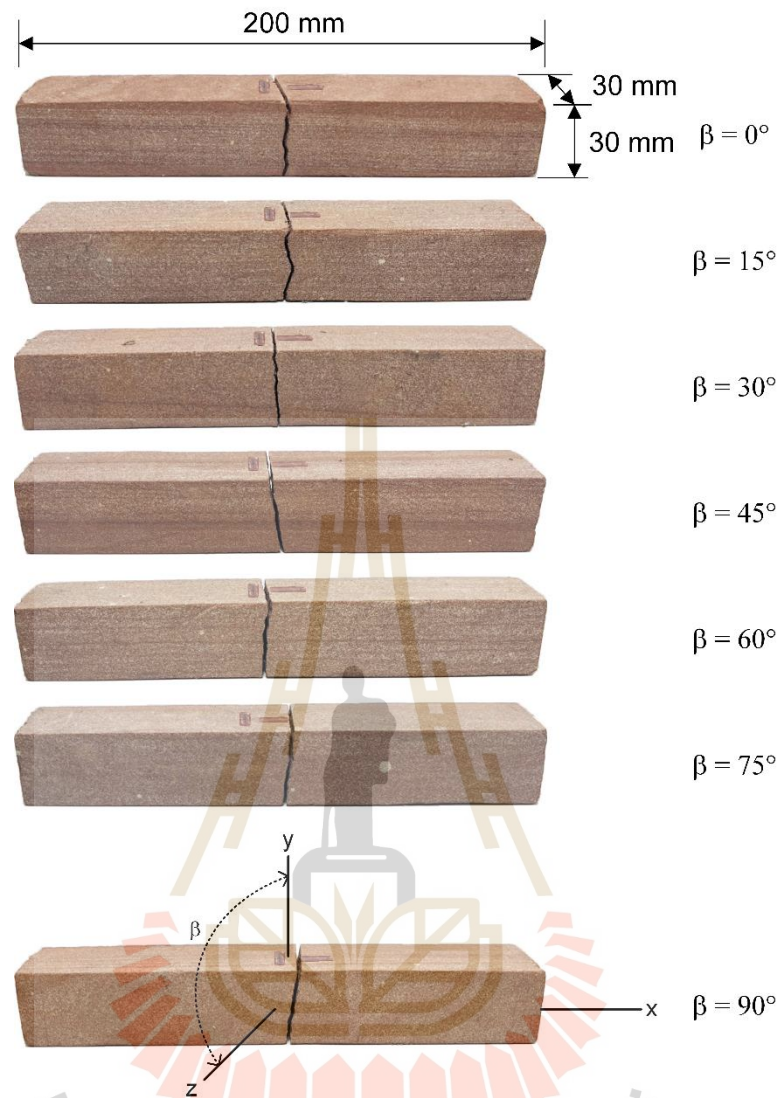


Figure 5.10 Post-test specimens for case 1 under bedding plane angles vary from $\beta = 0^\circ$ to 90° .

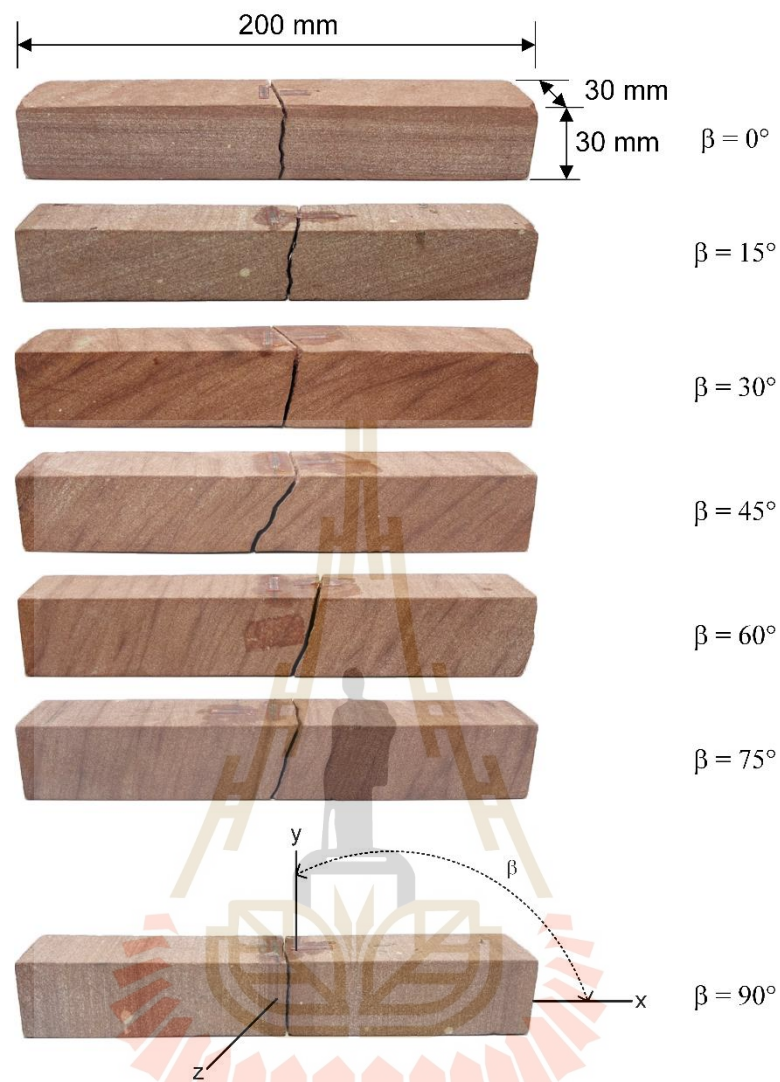


Figure 5.11 Post-test specimens for case 2 under bedding plane angles vary from $\beta = 0^\circ$ to 90° .

CHAPTER 6

ANALYSIS OF TEST RESULTS

6.1 Introduction

This chapter describes analysis of results obtained from four-point bending test. The objective of this analysis is to determine deformability under transverse isotropic are compared to the Amadei's solution. Both elastic moduli and Poisson's ratios are analyzed.

6.2 Amadei's solution

The intrinsic and apparent elastic moduli and Poisson's ratios are compared with Amadei (1996) solution who presents the theoretical prediction for deformability of anisotropic rocks. Amadei's solutions have been widely used on various anisotropic rock (Amadei, 1996; Cho et al., 2012; Yun-si et al., 2012; Gholami and Rasouli, 2014; Sukjaroen et al., 2021; Thongprapha et al., 2022). The required results for the calculation are the intrinsic elastic parameters for bedding plane angles β of 0° and 90° . The intrinsic elastic parameters from the test results are shown in Table 6.1. Based on generalized Hook's law, Amadei (1996) offers two variables for Young's modulus and Poisson's ratio of transverse isotropic material which can be calculated as:

$$E_y = 1/a_{22} \quad (6.1)$$

$$\nu_{yz} = a_{23}/a_{22} \quad (6.2)$$

where E_y is apparent Young's modulus in x, y and z coordinate systems, ν_{yz} is Poisson's ratio on y-z plane, and a_{22} and a_{23} are compliance components. These components can be obtained as follows:

$$a_{22} = \cos^4\beta/E' + \sin^4\beta/E + \sin^2 2\beta/4(1/G' - 2\nu'/E') \quad (6.3)$$

$$a_{23} = (\nu'/E')\cos 2\beta - (\nu/E)\sin^2\beta \quad (6.4)$$

where E and E' are intrinsic Young's moduli parallel and normal to bedding plane orientation, respectively, ν and ν' are intrinsic Poisson's ratios characterizing the lateral strain response on bedding plane parallel and normal to loading direction, G' is the shear modulus on normal to the transverse isotropy plane, and G is the shear modulus on bedding plane. These shear modulus parameters are determined, as follows:

$$1/G' = 1/E + 1/E' + 2\nu'/E' \quad (6.5)$$

$$1/G = E/(2(1+\nu)) \quad (6.6)$$

The intrinsic elastic parameters in Table 6.1 are substituted into equations (6.3) and (6.4). Substituting these compliance components into equations (6.1) and (6.2), the apparent elastic moduli and Poisson's ratios under different bedding plane orientations can be determined.

Figure 6.1 shows polar plots comparing the apparent elastic moduli (data points) with Amadei's predicted lines under different bedding plane angles for case 1. The apparent compressive elastic and tensile moduli under transverse isotropic effect show the shape as an ellipse. The apparent compressive elastic moduli are higher than those under tension. The maximum apparent elastic moduli are observed for bedding plane parallel to loading direction.

Figure 6.2 shows polar plots of the apparent elastic moduli and Amadei's predicted lines under different bedding plane angles for case 2. The apparent elastic moduli for both conditions are highest when bedding plane is normal to loading direction. The elliptical shape under compression is larger than those under tension, suggesting that Young's moduli under compression are always greater than those under tension.

Table 6.1 Intrinsic elastic parameters for both cases.

Case	Type of stress	E (GPa)	E' (GPa)	ν	ν'	G (GPa)	G' (GPa)
Case 1	Compression	13.30	10.69	0.20	0.23	5.47	4.71
	Tension	8.49	7.11	0.07	0.08	3.94	3.55
Case 2	Compression	9.17	10.69	0.26	0.23	3.68	4.06
	Tension	4.15	7.11	0.12	0.08	1.88	2.47

The apparent Poisson's ratios on y-z plane (ν_{yz}) under compression and tension for case 1 are shown in Figure 6.3. The diagram presents in the form of polar plots comparing between data points and Amadei's predicted line. The Poisson's ratios under tensile stress are less than half of those measured under compressive stress. Both cases show similar Poisson's ratio values. Poisson's ratios are greatest at $\beta = 0^\circ$ and lowest at $\beta = 90^\circ$. The bedding plane angle (β) has small effect on the Poisson's values.

Figure 6.4 presents the apparent Poisson's ratios on y-z plane (ν_{yz}) under compression and tension for case 2. The Poisson's ratios are highest at $\beta = 90^\circ$ and slightly decrease to $\beta = 0^\circ$. Poisson's ratios for case 2 are larger than those for case 1.

The mean misfit can be used to evaluate the discrepancy between the test results and Amadei's prediction. The mean misfit (s_i) is calculated as follows (Riley et al., 1998):

$$s_i = [(1/n) (\sum_{j=1}^n (X_{j,p} - X_{j,t})^2)]^{1/2} \quad (6.7)$$

where $X_{j,p}$ and $X_{j,t}$ are the predicted and measured apparent elastic moduli or Poisson's ratios, and n is the number of bedding plane angles (β). The mean misfit for apparent tensile and compressive elastic moduli are 0.42, 0.51 GPa for case 1, and 0.23, and 0.29 GPa for case 2. For the apparent Poisson's ratios under tension and compression s_i values are 0.005, 0.007 for case 1, and 0.005, and 0.005 for case 2. The low values of mean misfit suggest that the Amadei's predictions agree well with the test results.

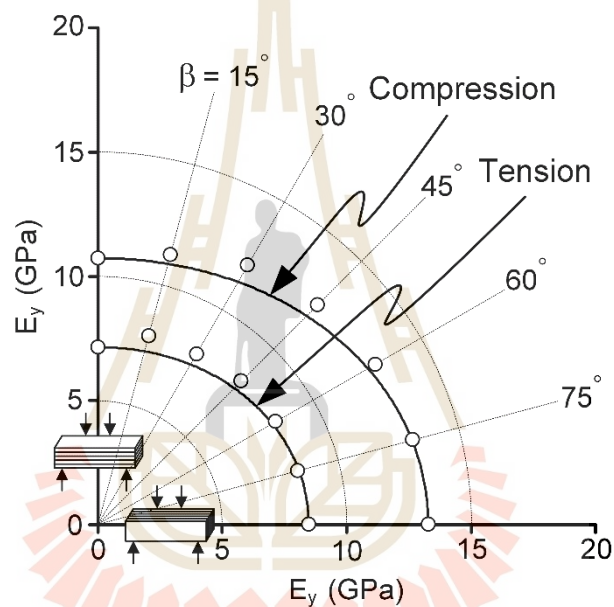


Figure 6.1 Polar plots of apparent elastic moduli under tension and compression for case 1.

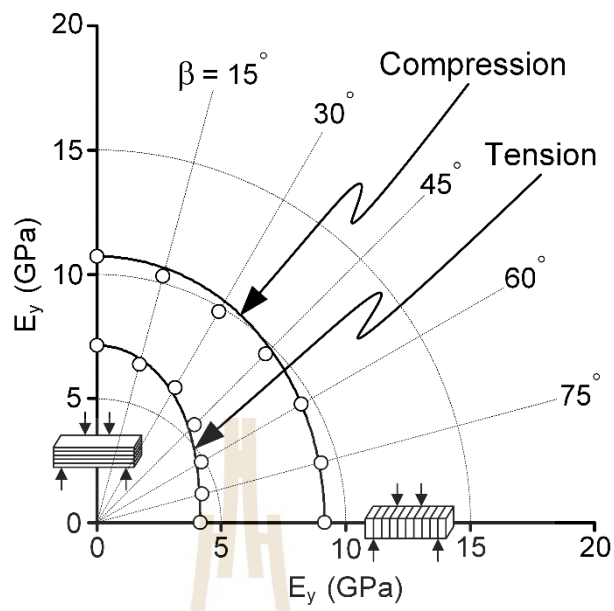


Figure 6.2 Polar plots of apparent elastic moduli under tension and compression for case 2.

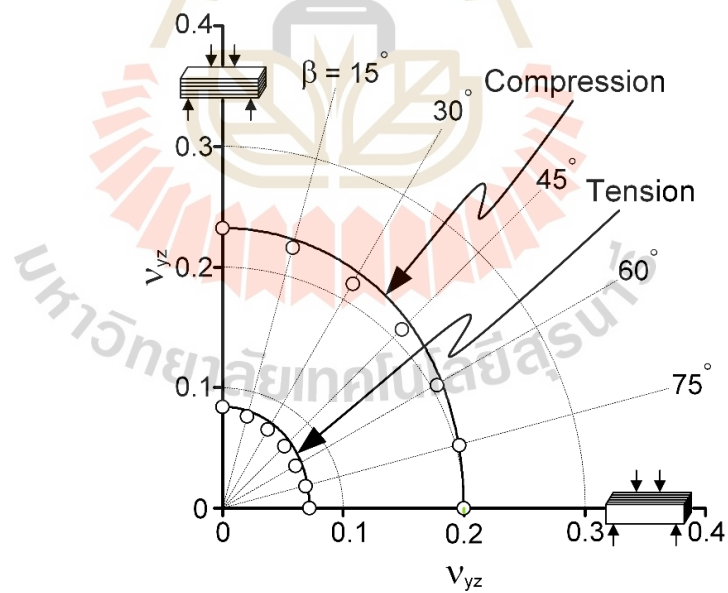


Figure 6.3 Polar plots of apparent Poisson's ratios under compression and tension for case 1.

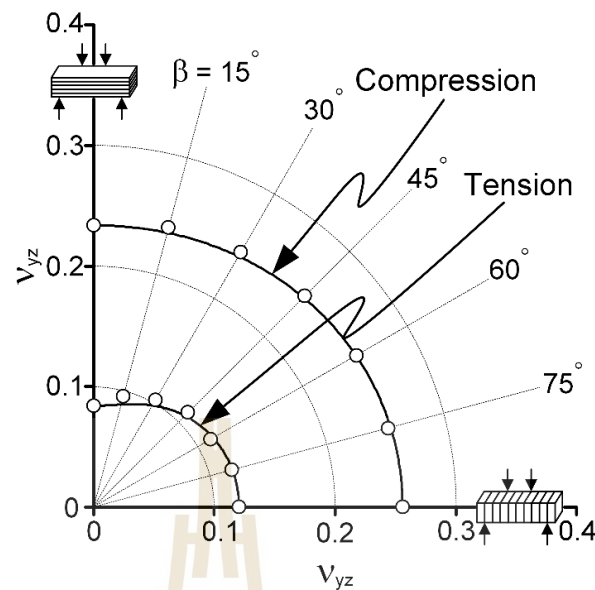


Figure 6.4 Polar plots of apparent Poisson's ratios under compression and tension for case 2.

6.3 Degrees of rock anisotropy

The degree of anisotropy of rock is determined by the maximum and minimum tensile strength ratio and maximum to minimum intrinsic elastic moduli ratio. The maximum to minimum parameters can be measured normal and parallel to bedding plane orientation. Several researchers (Ramamurthy, 1993; Ma et al., 2018) have study ratio of rock anisotropy both tensile strength and elastic modulus. Ramamurthy (1993) suggests that the degree of anisotropy is normally in the range of 1 to 6, where each degree indicates the quality of anisotropic rock, such as low (1.1-2.0), medium (2.0-4.0), high (4.0-6.0), and very high anisotropy (more than 6). The rock is under isotropic effect where the degree of anisotropy is equal to 1-1.1. Table 6.2 shows degree of anisotropy of tensile strength for both cases. The degrees of anisotropy on tensile strength of Phu Phan sandstone are shown in Figure 6.5. The diagram shows that each straight line has slopes of 1, 2, 3, and 4. The results of this study for both cases show low anisotropy because they ranged from 1 to 2. For case 1, degree of anisotropy under tension is slightly lower than that for case 2.

Table 6.3 shows degree of anisotropy for elastic moduli. The results obtained from elastic moduli under compression and tension for both cases are shown in Figure

6.6. The open data points represent the tensile elastic modulus. Compressive elastic modulus is presented by a rectangular symbol. They indicate that the degrees of anisotropy in terms of elastic moduli under compression and tension for both cases are low, ranging from 1 to 2. Degree of anisotropy is highest under tensile conditions for case 1. The lowest degree of anisotropy is found from elastic modulus under compression for case 2.

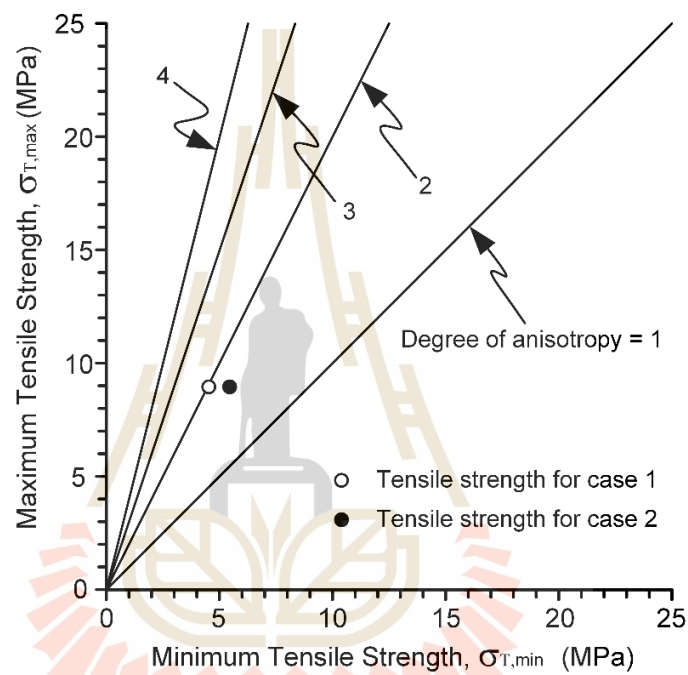


Figure 6.5 Relationship between maximum tensile strength ($\sigma_{T,max}$) and minimum tensile strength ($\sigma_{T,min}$) of Phu Phan sandstone.

Table 6.2 Degree of anisotropy on tensile strength for Phu Phan sandstone.

Case	Tensile strength (MPa)		Degree of anisotropy
Case 1	$\sigma_{T,max}$	8.93	1.63
	$\sigma_{T,min}$	5.48	
Case 2	$\sigma_{T,max}$	8.93	1.96
	$\sigma_{T,min}$	4.56	

Table 6.3 Degree of anisotropy on compressive and tensile elastic moduli of Phu Phan sandstone.

Case	Elastic moduli			Degree of anisotropy
Case 1	Compressive elastic moduli, (GPa)	$E_{C,max}$	13.30	1.24
		$E_{C,min}$	10.69	
	Tensile elastic moduli, (GPa)	$E_{T,max}$	8.49	1.19
		$E_{T,min}$	7.11	
Case 2	Compressive elastic moduli, (GPa)	$E_{C,max}$	10.69	1.17
		$E_{C,min}$	9.17	
	Tensile elastic moduli, (GPa)	$E_{T,max}$	7.11	1.72
		$E_{T,min}$	4.15	

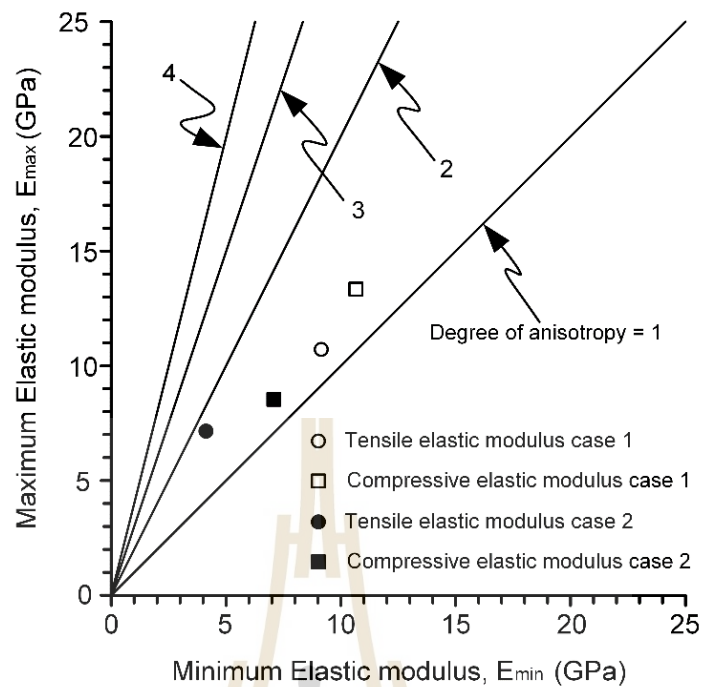


Figure 6.6 Relationship between maximum elastic modulus (E_{max}) and minimum elastic modulus (E_{min}) under compression and tension for both cases.

6.4 Transversely isotropy effect on tensile strength

The tensile strength results under transversely isotropic effect in previous chapter are described to compare various tensile test obtained elsewhere. The various tensile tests consist of three-point bending test, direct tensile test, Brazilian test, and ring test. The results in this study indicate that the bending tensile strength decreases as bedding plane orientations rotate toward loading direction. The highest tensile strength occurs when bedding planes are parallel to induced tensile stress at $\beta = 0^\circ$ and lowest value as they are normal to induced stress at $\beta = 90^\circ$. The tensile strengths under transversely isotropic effect compared with various test methods are shown in Figure 6.7. The tensile strengths for this study are similar to results from several researchers (Dou et al., 2019; Huang et al., 2020 on three-point bending test, Nova and Zaninetti, 1990; Lee and Pietruszczak, 2015; Shang et al., 2018 on direct tension test, Zhong et al., 2020; Xiao-jing et al., 2016; Suwankeeree, 2021 on Brazilian test, and Chen and Hsu, 2001 on ring test). This diagram also shows each test method gives different tensile strengths. The ring test shows higher tensile strength than other tensile test

methods. Brazilian and direct tensile tests have relatively low tensile strengths. For bending test (three- and four-point bending), the values give slightly higher than those from Brazilian test.

Four-point bending tensile strengths for this study are compared with previous results obtained from Brazilian test of Suwankeeree (2021), who study transversely isotropic effect on Brazilian tensile strength of bedded sandstone. Sandstone specimens are selected for the same formation. Figure 6.8 shows tensile strength comparing between four-point bending and Brazilian tests of Phu Phan sandstone. The results for both methods observe that the decrease of tensile strength occur when bedding plane angles increase. Bending tensile strengths for this study are higher than those the results obtained from Brazilian test. Brazilian tensile strengths are about 47.47-53.90% for case 1 and 48.96-64.77% for case 2 of bending tensile strengths for this study. Tensile strength results for both tests are summarized in Table 6.4.

Several researchers study three orientations of bedding plane on maximum load from bending test. The orientations of bedding plane are divided into 3 types: 1) bedding planes normal to loading direction, 2) bedding planes parallel to main axis, and 3) bedding planes parallel to loading direction. Figure 6.9 shows a comparison of maximum loads of three bedding plane orientations in the form of bar charts. This chart shows that the maximum load is highest when bedding plane normal to loading direction. Bedding plane parallel to loading direction gives the lowest value. For bedding plane parallel to main axis, the values are lower than that for type 1 and higher than that for type 3. The results for this study tend to be similar to those of Heng et al. (2020), Ren et al. (2021), Wu et al. (2017), Kramarov et al. (2020), and Li et al. (2019). All results for this study and several researchers are summarized in Table 6.5

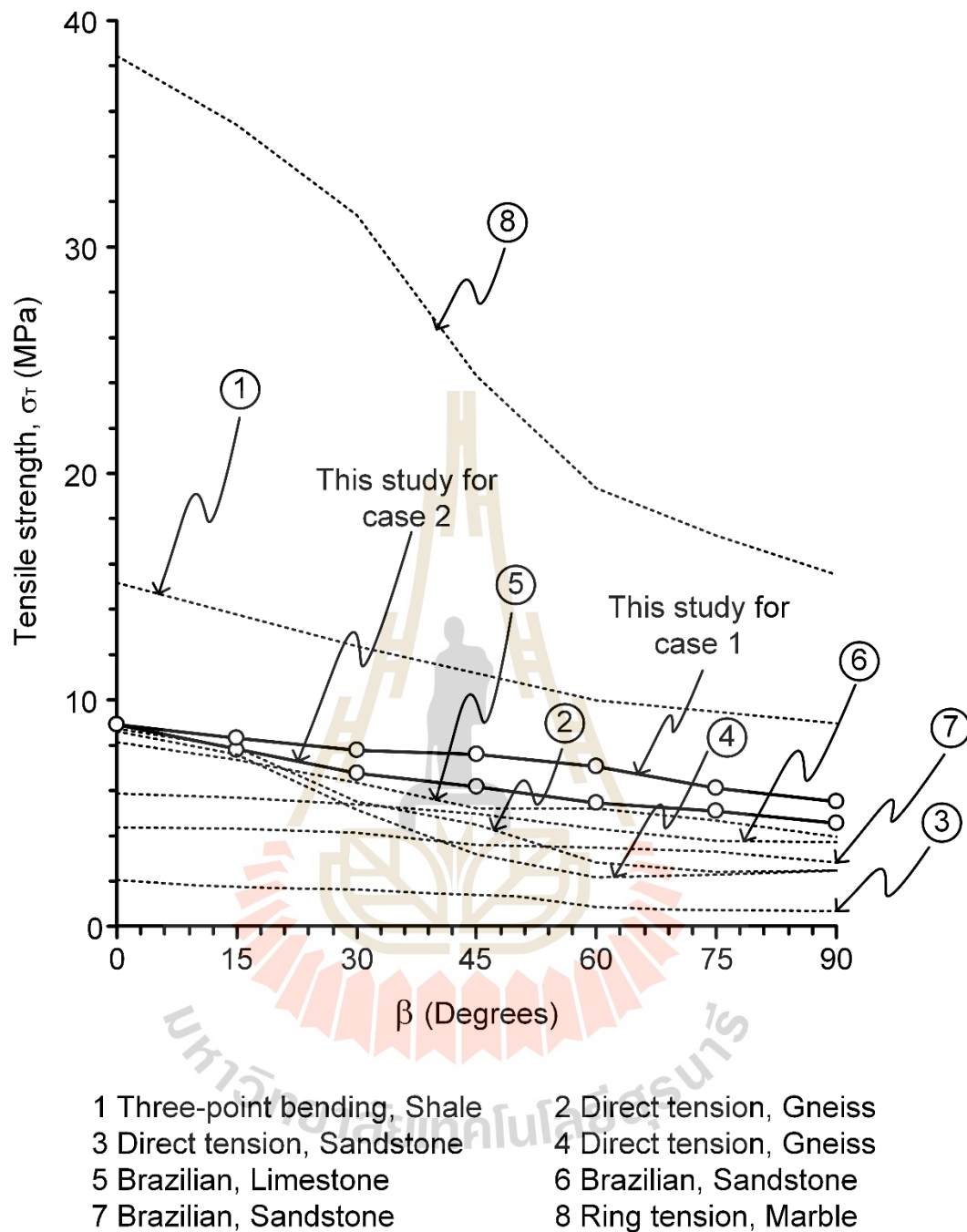


Figure 6.7 Tensile strengths as a function of bedding plane angle compared to those of ① Dou et al. (2019), ② Nova and Zaninetti (1990), ③ Lee and Pietruszczak (2015), ④ Shang et al. (2018), ⑤ Zhong et al. (2020), ⑥ Xiaojing et al. (2016); ⑦ Suwankeeree (2021), and ⑧ Chen and Hsu (2001).

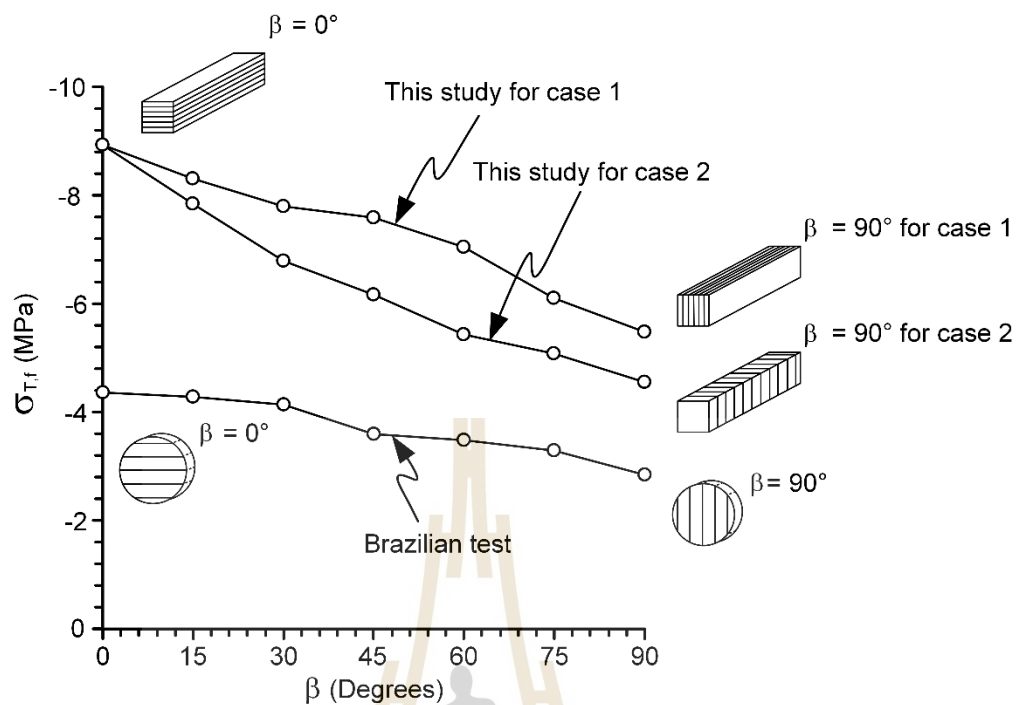


Figure 6.8 Tensile strengths of Phu Phan sandstone as a function of bedding plane angle compared between four-point bending and Brazilian tests.

Table 6.4 Tensile strengths of Phu Phan sandstone from four-point bending and Brazilian test results.

β (degrees)	Tensile strength of Phu Phan sandstone (MPa)		
	This study for case 1	This study for case 2	Suwankeeree (2021)
0	8.93	8.93	4.37
15	8.31	7.84	4.29
30	7.80	6.80	4.14
45	7.58	6.17	3.6
60	7.05	5.44	3.49
75	6.10	5.08	3.29
90	5.48	4.56	2.85

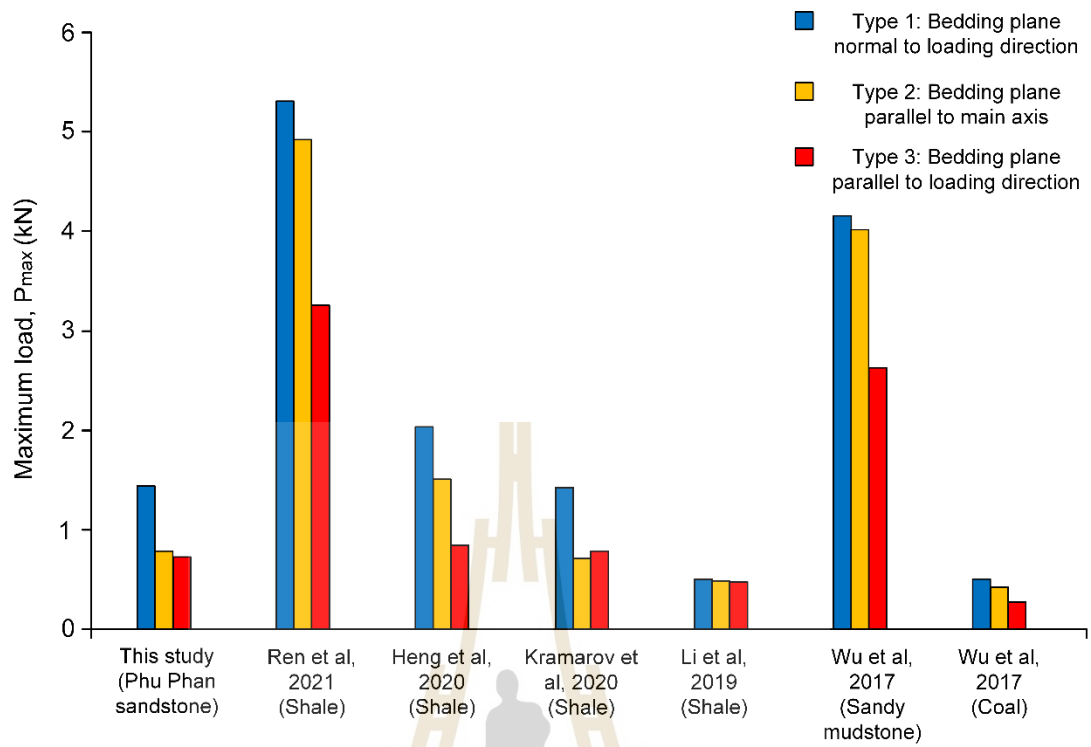


Figure 6.9 Comparison of maximum loads under three orientations of bedding plane.

Table 6.5 Summary of maximum load under three orientations of bedding plane.

Type of testing	Rock type	Maximum load (kN)			References
		Type 1	Type 2	Type 3	
Four-point bending	Phu Phan sandstone	1.432	0.7876	0.716	This study
Three-point bending	Silurian Longmaxi Shale	2.032	1.512	0.843	Heng et al., 2020
	Silurian Longmaxi Shale	5.306	4.919	3.258	Ren et al., 2021
	Marcellus shale	0.5036	0.498	0.473	Li et al, 2019
Semicircular three-point bending	Sandy mudstone	4.160	4.023	2.630	Wu et al., 2017
	Coal	0.500	0.430	0.272	Wu et al., 2017
	Mancos Shale	1.423	0.721	0.783	Kramarov et al., 2020

CHAPTER 7

DISCUSSIONS AND CONCLUSIONS

7.1 Discussions

Tensile strength and elastic properties of transversely isotropic sandstone are studied by using four-point bending test. Phu Phan sandstones are selected and prepared under different bedding plane orientations. The elastic properties of transversely isotropic rock are compared with Amadei's solution.

The test results indicate that the maximum bending tensile strength occurs when bedding planes are parallel to the induced tensile stresses. The minimum tensile strength is observed when bedding planes are normal to tensile strength. This is because bedding planes normal is more easily separated under tension. The results tend to be similar to various tension methods performed elsewhere by Dou et al. (2019) on Longmaxi shale; Huang et al. (2020) on sandstone for three-point bending test, Zhong et al. (2020) on layered limestone; Xiao-jing et al. (2016) on Bedded sandstone; Suwankeeree (2021) on Phu Phan sandstone for Brazilian test, Nova and Zaninetti (1990) on quartzitic gneiss; for direct tension test, and Chen and Hsu (2001) on Hualian marble for ring test.

The tensile strengths as a function of bedding plane orientation from this study are compared with various tensile tests by several researchers as shown in Figure 6.7. The ring test by Chen and Hsu (2001) provides the highest strength because the stress gradient of ring test occurs along the incipient crack plane (Fuenkajorn and Klanphumeesri, 2010). Brazilian and direct tensile tests show relatively low tensile strengths as shown by Nova and Zaninetti (1990), Lee and Pietruszczak (2015), Shang et al. (2018), Zhong et al. (2010), Xiao-jing et al. (2016); Suwankeeree (2021). Three (Dou et al., 2019) and four-point bending (This study) give tensile strengths slightly higher than those from Brazilian and direct tension tests but they are lower than that ring test. This is because the stress gradient for each method differs around the area that is subjected to the maximum tensile stress (Kear and Bungler, 2014). For Brazilian and

direct tension tests, high stress gradients under tension regularly distribute at mid-section on center of specimen. Three and four-point bending test shows highest stress gradient at mid-section of the specimen, they give greater tensile strength than those of Brazilian and direct tension methods. As a result of Suwankeeree (2021) clearly shows that sandstone in identical formation, Brazilian tensile strengths for all bedding plane angles are lower than those four-point bending tensile strength for this study. The different tensile strengths from various tests have been observed by Liao et al. (2019) and Efe et al. (2019), who conclude that tensile strength of bending test is highest among those of Brazilian and direct tension tests. Three-point bending test is higher than four-point bending test. This is due to maximum three-point bending tensile strength that occurs at mid-section. For four-point bending test, maximum tensile strength induces between two loading points (Hein and Brancheriau, 2018). Each method gives different values because ring, Brazilian, and direct tension tests that tensile strengths are dependent on specimen shape (Coviello et al., 2005).

Bending tensile strength for case 1 (bedding plane strikes parallel to induce tensile stress) is lower than that at $\beta = 0^\circ$ (bedding plane parallel to the tensile strength) and higher than that for case 2 at $\beta = 90^\circ$ (bedding plane normal to the tensile strength). This is because the fracture can dilate easily along bedding plane and pore space of rock. This result tends to be similar to those obtained from Pires et al. (2011) on slate for four-point flexural, Wu et al. (2017) on mudstone and coal; Li et al. (2019); Kramarov et al. (2020); Heng et al. (2020); Ren et al. (2021) on Shale for three-point bending test. They postulate that the that maximum bending tensile strength occurs where induced tensile strength parallel to bedding plane. Bedding plane normal to induce tensile strength gives lower value than that parallel to it.

The elastic moduli under tension for case 1 are largest when the induced tensile stress is parallel to bedding plane strike (Figure 5.1). When the induced tensile stress is normal to bedding planes (Figure 5.3), the tensile moduli are lowest as the beds can be separated more easily. This is because strains elongate and contract well when bedding plane strikes parallel to induced stress. The compressive elastic moduli for both cases tend to show similar behavior with those under tension.

Both elastic moduli and Poisson's ratios under tension are lower than those under compression. This is because the pore spaces and fissures in the rock easily dilate in the directions normal to bedding plane (Figure 5.6 and 5.7). The results obtained here agree reasonably well with those obtained by Fuenkajorn and Klanphumeesri (2010) on sandstone, marble, and limestone, Stimpson and Chen (1993) on halite, potash, limestone, and granite, who conclude that the elastic parameters under tension are significantly lower than those under compression. The difference between elastic moduli under both conditions depends on the pore space of rock, micro-fissures, and the bond strength of cementing materials and inter-crystalline boundaries.

The apparent elastic moduli for both conditions agree well with Amadei's prediction. Different bedding plane orientations have slight effect on apparent Poisson's ratios on y-z plane (ν_{yz}) under tension and compression. The apparent elastic moduli and Poisson's ratios under tension are lower than those under compression. The low mean misfit values between Amadei's predicted line and test data suggest that they are in close agreement.

The degree of anisotropy of Phu Phan sandstone in the form of maximum to minimum tensile strength and elastic modulus ratios are in the range of 1-2. Phu Phan sandstone is considered low anisotropy based on classification of anisotropy by Ramamurthy (1993).

7.2 Conclusions

The effect of transverse isotropy on tensile strength and elastic properties of Phu Phan sandstone is studied by performing four-point bending test, based on generalized Hooke's law. The findings can be summarized as follows.

1) Bending tensile strength is largest of 8.93 MPa when bedding planes are parallel to induced tensile stress. The lowest tensile strength of the sandstone occurs where bedding planes are normal to tensile stress and have a value equal to 4.56 MPa.

2) When induced tensile stresses parallel to bedding plane strike (case 1), bending tensile strengths for all bedding plane angles are greater than those of case 2.

3) The four-point bending results under transverse isotropy effect tend to be similar to various tension methods obtained elsewhere.

4) The induced tensile stress normal to bedding planes give lowest elastic moduli of 8.49 GPa. The highest elastic moduli are found when induced tensile stress parallel to bedding planes of 4.15 GPa. Poisson's ratios under both conditions seem to be insensitive to the bedding plane angle.

5) The elastic moduli and Poisson's ratios for both cases under tension are lower than those under compression.

6) The apparent elastic moduli and Poisson's ratios on y-z plane (\mathbf{V}_{yx}) from test data agree well with those predictions by Amadei's solution. The mean misfits for the apparent elastic parameters give low values.

7) The degree of anisotropy of Phu Phan sandstone used in this study is in the range of 1.63 and 1.96 for tensile strength and 1.17-1.72 for elastic moduli under both test conditions, which is classified as low anisotropy.

7.3 Recommendations for future studies

1) Sedimentary and metamorphic rock normally show bedding plane or foliation plane that should be considered to study mechanical properties on effect of transverse isotropic.

2) The effect of loading rate, specimen size, and saturated condition on bending tensile strength should be investigated on transverse isotropic rock.

3) Numerical simulation in the form of 3D should be studied to assess roof span stability of underground excavation under transverse isotropic effects in different axes.

REFERENCES

- Aliabadian, Z., Zhao, G. F., and Russell, A. R. (2019). Crack development in transversely isotropic sandstone discs subjected to Brazilian tests observed using digital image correlation. *International Journal of Rock Mechanics and Mining Sciences*. 119: 211-221.
- Amadei, B. (1996). Importance of anisotropy when estimating and measuring in situ stresses in rock. *International Journal of Rock Mechanics and Mining Sciences & Geomechanics Abstracts*. 33(3): 293-325.
- ASTM D6272-17 (2020). Standard test method for flexural properties of unreinforced and reinforced plastics and electrical insulating materials by four-point bending. *Annual Book of ASTM Standards*. American Society for Testing and Materials, West Conshohocken, PA.
- Berčáková, A., Melichar, R., Obara, Y., Ptáček, J., and Souček, K. (2017). Evaluation of anisotropy of fracture toughness in brittle rock, migmatized gneiss. *Procedia engineering*. 191: 900-907.
- Chen, C. S., and Hsu, S. C. (2001). Measurement of indirect tensile strength of anisotropic rocks by the ring test. *Rock mechanics and rock engineering*. 34(4): 293-321.
- Cho, J. W., Kim, H., Jeon, S., and Min, K. B. (2012). Deformation and strength anisotropy of Asan gneiss, Boryeong shale, and Yeoncheon schist. *International journal of rock mechanics and mining sciences*. 50: 158-169.
- Coviello, A., Lagioia, R. O. C. C. O., and Nova, R. O. B. E. R. T. O. (2005). On the measurement of the tensile strength of soft rocks. *Rock Mechanics and Rock Engineering*. 38: 251-273.
- Department of Mineral Resources (2007). Geological Map of Thailand 1:250,000. *Department of Mineral Resources, Ministry of Natural Resources and Environment*. Bangkok, Thailand.

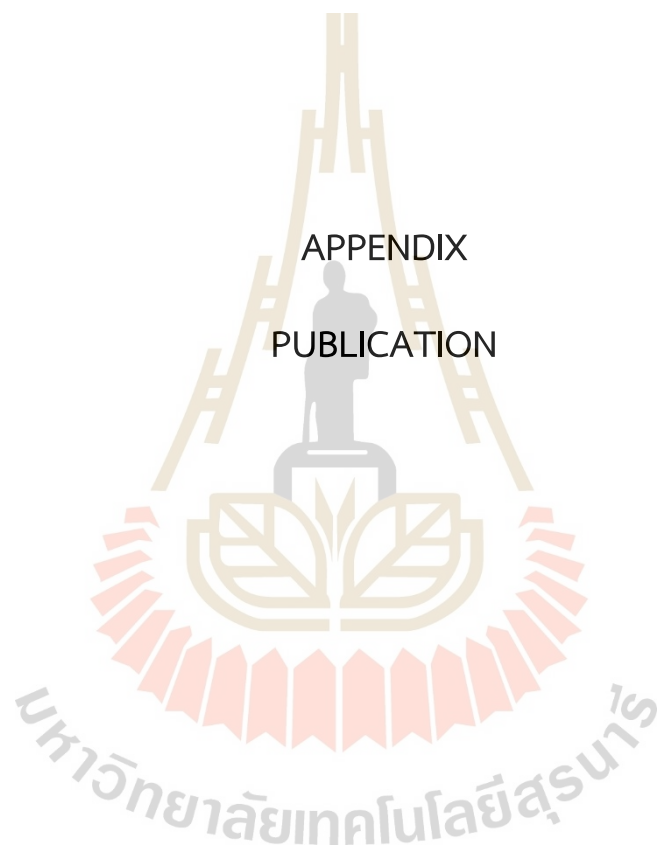
- Dou, F., Wang, J. G., Zhang, X., and Wang, H. (2019). Effect of joint parameters on fracturing behavior of shale in notched three-point-bending test based on discrete element model. *Engineering Fracture Mechanics*. 205: 40-56.
- Efe, T., Sengun, N., Demirdag, S., Tufekci, K., and Altindag, R. (2019). Effect of sample dimension on three and four points bending tests of fine crystalline marble and its relationship with direct tensile strength. *IOP Conference Series: Earth and Environmental Science*. 221(1): 012093.
- Fuenkajorn, K., and Klanphumeesri, S. (2010). Direct tension tests of intact rocks using compression-to-tension load converter. *Engineering Journal of Research and Development*. 21(2): 51-57.
- Gholami, R., and Rasouli, V. (2014). Mechanical and elastic properties of transversely isotropic slate. *Rock Mechanics and Rock Engineering*. 47(5): 1763-1773.
- Hakala, M., Kuula, H., and Hudson, J. A. (2007). Estimating the transversely isotropic elastic intact rock properties for in situ stress measurement data reduction: a case study of the Olkiluoto mica gneiss, Finland. *International Journal of Rock Mechanics and Mining Sciences*. 44(1): 14-46.
- Hein, P. R. G., and Brancheriau, L. (2018). Comparison between three-point and four-point flexural tests to determine wood strength of Eucalyptus specimens. *Maderas Ciencia y tecnología*. 20(3): 333-342.
- Heng, S., Li, X., Liu, X., and Chen, Y. (2020). Experimental study on the mechanical properties of bedding planes in shale. *Journal of Natural Gas Science and Engineering*. 76: 103161.
- Huang, D., Li, B., Ma, W. Z., Cen, D. F., and Song, Y. X. (2020). Effects of bedding planes on fracture behavior of sandstone under semi-circular bending test. *Theoretical and Applied Fracture Mechanics*. 108: 102625.
- Kear, J., and Bungler, A. P. (2014). Dependence of static fatigue tests on experimental configuration for a crystalline rock. *Advanced Materials Research*. 891: 863-871.
- Khanlari, G. R., Heidari, M., Sepahigero, A. A., and Fereidooni, D. (2014). Quantification of strength anisotropy of metamorphic rocks of the Hamedan province, Iran, as determined from cylindrical punch, point load and Brazilian tests. *Engineering Geology*. 169: 80-90.

- Kramarov, V., Parrikar, P. N., and Mokhtari, M. (2020). Evaluation of fracture toughness of sandstone and shale using digital image correlation. *Rock Mechanics and Rock Engineering*. 53: 4231-4250.
- Lee, Y. K., and Pietruszczak, S. (2015). Tensile failure criterion for transversely isotropic rocks. *International Journal of Rock Mechanics and Mining Sciences*. 79: 205-215.
- Li, W., Jin, Z., and Cusatis, G. (2019). Size effect analysis for the characterization of marcellus shale quasi-brittle fracture properties. *Rock Mechanics and Rock Engineering*. 52: 1-18.
- Liao, J. J., Yang, M. T., and Hsieh, H. Y. (1997). Direct tensile behavior of a transversely isotropic rock. *International Journal of Rock Mechanics and Mining Sciences*. 34(5): 837-849.
- Liao, Z. Y., Zhu, J. B., and Tang, C. A. (2019). Numerical investigation of rock tensile strength determined by direct tension, Brazilian and three-point bending tests. *International Journal of Rock Mechanics and Mining Sciences*. 115: 21-32.
- Ma, T., Peng, N., Zhu, Z., Zhang, Q., Yang, C., and Zhao, J. (2018). Brazilian tensile strength of anisotropic rocks: review and new insights. *Energies*. 11(2): 304.
- Nova, R., and Zaninetti, A. (1990). An investigation into the tensile behaviour of a schistose rock. *International Journal of rock mechanics and mining sciences & geomechanics abstracts*. 27(4): 231-242.
- Pires, V., Amaral, P. M., Rosa, L. G., and Camposinhos, R. S. (2011). Slate flexural and anchorage strength considerations in cladding design. *Construction and Building Materials*. 25(10): 3966-3971.
- Plangklang, J., Artkhonghan, K., Tepnarong, P., and Fuenkajorn, K. (2017). Time-dependent tensile strength of maha sarakham salt. *Engineering Journal of Research and Development*. 28(4): 5-12.
- Racey, A. (2009). Mesozoic red bed sequences from SE Asia and the significance of the Khorat Group of NE Thailand. *Geological Society, London, Special Publications*. 315(1): 41-67.
- Ramamurthy, T., Rao, G. V., and Singh, J. (1993). Engineering behaviour of phyllites. *Engineering Geology*. 33(3): 209-225.

- Ren, L., Xie, H. P., Sun, X., Zhang, R., Li, C. B., Xie, J., and Zhang, Z. T. (2021). Characterization of anisotropic fracture properties of Silurian Longmaxi shale. *Rock Mechanics and Rock Engineering*. 54: 665-678.
- Riley, K. F., Hobson, M. P., and Bence, S. J. (1999). *Mathematical methods for physics and engineering*.
- Shang, J., Duan, K., Gui, Y., Handley, K., and Zhao, Z. (2018). Numerical investigation of the direct tensile behaviour of laminated and transversely isotropic rocks containing incipient bedding planes with different strengths. *Computers and Geotechnics*. 104: 373-388.
- Singh, J., Ramamurthy, T., and Venkatappa Rao, G. (1989). Strength anisotropies in rocks. *Indian Geotechnical Journal*. 19(2): 147-166.
- Stimpson, B., and Chen, R. (1993). Measurement of rock elastic moduli in tension and in compression and its practical significance. *Canadian Geotechnical Journal*. 30(2): 338-347.
- Sui, W., Wang, Y., and Li, J. (2023). Microscopic Study of Shale Anisotropy with SEM In Situ Compression and Three-Point Bending Experiments. *Energies*. 16(5): 2440.
- Sukjaroen, N., Thongprapha, T., Liabkrathok, P., and Fuenkajorn, K. (2021). Effects of loading rate on transverse isotropic responses of bedded gypsum. *Arabian Journal of Geosciences*. 14: 1-13.
- Suwankeeree, S. (2021). Effect of transverse isotropy on tensile strength and deformability of sandstone. *Master thesis*. Suranaree University of Technology, Nakhon Ratchasima.
- Tavallali, A., and Vervoort, A. (2010). Effect of layer orientation on the failure of layered sandstone under Brazilian test conditions. *International journal of rock mechanics and mining sciences*. 47(2): 313-322.
- Thongprapha, T., Tengpakwaen, K., Daemen, J. J. K., and Fuenkajorn, K. (2022). Effect of confining pressures on transverse isotropy of Maha Sarakham salt. *International Journal of Rock Mechanics and Mining Sciences*. 152: 105077.
- Veeravinantanakul, A., Kanjanapayont, P., Sangsompong, A., Hasebe, N., and Charusiri, P. (2018). Structure of Phu Phan Range in the Khorat Plateau: Its Apatite Fission

- Track Ages and Geological Syntheses. *Bulletin of Earth Sciences of Thailand*. 10(1): 8-16.
- Vervoort, A., Min, K. B., Konietzky, H., Cho, J. W., Debecker, B., Dinh, Q. D., and Tavallali, A. (2014). Failure of transversely isotropic rock under Brazilian test conditions. *International Journal of Rock Mechanics and Mining Sciences*. 70: 343-352.
- Wu, P. F., Liang, W. G., Li, Z. G., Cao, M. T., and Yang, J. F. (2017). Investigations on mechanical properties and crack propagation characteristics of coal and sandy mudstone using three experimental methods. *Rock Mechanics and Rock Engineering*. 50: 215-223.
- Xiao-jing, Z., Hua-feng, D., Heng-bin, Z., Chenxie-jie, W., Jing-cheng, F., Yao, X., and Yu, H. (2016). The Influence of Bedding Angle on the Tensile Strength and Failure Mode of Bedded Sandstone. *Electronic Journal of Geotechnical Engineering*. 21: 5547-5558.
- Yun-si, L., Xiao, Z., and Quan, Y. (2012). The five elastic parameters for the anisotropy of slate under the influence of different bedding orientations. *Electron Journal of Geotechnical Engineering*. 17: 3695-3707.
- Zhong, S., Zuo, S. Y., Mao, L., Luo, S., and Wang, X. J. (2020). Mechanism of anisotropic characteristics of layered limestone and a constitutive model for different bedding angles based on a Brazilian tensile test. *Arabian Journal of Geosciences*. 13: 1-9.

APPENDIX
PUBLICATION



LIST OF PUBLICATION

Jakkawachote, S. and Fuenkajorn, K. (2022). Effect of transverse isotropy on tensile strength and elastic properties of Phu Phan sandstone by four-point bending test. In Proceedings of Academicsera International Conference, 25th - 26th December, 2022 (pp. 1-6). Macau, China.



EFFECT OF TRANSVERSE ISOTROPY ON TENSILE STRENGTH AND ELASTIC PROPERTIES OF PHU PHAN SANDSTONE BY FOUR-POINT BENDING TEST

¹SUJINDA JAKKAWACHOTE, ²KITTITTEP FUENKAJORN

Geomechanics Research Unit, Institute of Engineering, Suranaree University of Technology, Nakhon Ratchasima, Thailand
E-mail: ¹sujinda.b5911356@gmail.com

Abstract - Four-point bending tests have been performed on prismatic block specimens of bedded sandstone under various bedding plane orientations. Rock specimens are prepared from Phu Phan formation to obtain nominal dimensions of 30×30×200 mm³. Bedding orientations (β) are separated into two cases; 1) beds are parallel to main axis, and 2) beds are normal to main axis. The results indicate that the transverse isotropic effect under tension occurs where tensile strength is lowest when normal to bedding planes makes an angle of 90° with loading direction and they gradually increase to the highest when $\beta = 0^\circ$. The elastic moduli and Poisson's ratios under tension are lower than those under compression. The elastic parameters are compared with those obtained from Amadei's solution. The findings can be used to predict tensile strength of sandstone under various bedding orientations and to design the maximum unsupported roof span of underground opening.

Keywords - Bedding Plane, Four-Bending Test, Elastic Modulus, Poisson's Ratio.

I. INTRODUCTION

Sedimentary and metamorphic rocks normally show well-defined structures in the form of bedding plane, foliation, jointing or fissuring [1]. Different orientations of bedding plane have influences on rock strength and elastic properties. In underground openings, rock tensile strength dictates the maximum roof span and its stability. Tensile strength is usually obtained from Brazilian tension test, direct tension test, ring tension test, and bending test. Four-point bending test is however more appropriate for roof span analysis because stress pattern is similar to that of roof span in underground opening [2]. Several researchers suggest that the tensile strength of transverse isotropic rocks changes with bedding plane orientations.

This agrees with the method obtained by Dou et al. [3] on three-point bending test, Aliabadian et al. [4], Suwankeeree [5] on Brazilian test, Liao et al. [6] on direct tensile test, and Chen and Hsu [7] on indirect tensile test. Pires et al. [8] perform four-point flexural tests on three different orientations of anisotropic planes. Their results indicate that flexural tensile strength for bedding plane normal to the loading direction is higher than those when bedding planes are parallel to the loading direction. Fuenkajorn and Klanphumeesri [9] show that elastic moduli and Poisson's ratios under tension of marble and sandstone tend to give lower values than those under compression. Thongprapha et al. [10], Hakala et al. [11] analyze and compare transverse isotropic materials with Amadei's solution. They conclude that the test results agree well with Amadei's predictions.

The effect of transverse isotropy on tensile strength and elastic parameters on rock under four-point bending test has rarely been studied. For underground opening, these knowledge's are needed for the analysis and design of roof span under transverse

isotropy effect. The objective of this study is to determine tensile strength and elastic properties of bedded sandstone based on four-point bending test. The properties are determined under various bedding plane orientations. The findings can be used to predict the maximum tensile strength of sandstone forming opening roof as affected by transverse isotropic planes.

II. ROCK SAMPLES

Test specimens are prepared from Phu Phan sandstone formation. They are cut to obtain prismatic blocks with nominal dimensions of 30 mm thick, 30 mm wide, and 200 mm long. Bedding plane orientations are arranged for two configurations: 1) bedding planes parallel to the main axis (Fig.1a) and 2) bedding planes normal to the main axis (Fig.1b). For the first case, the beds are rotated around x-axis (main axis).

The second case shows the beds rotating around z-axis. Bedding orientations (β) are varied from 0, 15, 30, 45, 60, 75 to 90 degrees. These angles (β) represent the angle between the normal to bedding plane and the loading direction. A total of 14 specimens have been prepared. X-ray diffraction analysis gives rock mineral compositions as 67.69% quartz, 11.50% oligoclase, 8.26% albite, 5.58% chlorite, 3.35% microcline, 2% anorthite, 1.11% calcite, 0.25% muscovite and 0.25 % kaolinite. The average density is 2.33±0.03 g/cm³. The bedding planes can be visually observed by gradations of quartz grains and alternating between light and dark brown color.

III. TEST APPARATUS AND METHOD

Test method and calculation for four-point bending test follow ASTM D6272-17 [12] standard.

Specimens are placed on the lower steel bars with two 25 mm diameter steel bases arranged for 240 mm spacing. The upper steel base is equipped with a load span of 60 mm (one-third of support span). Loading

is applied to the specimens through a spherical bearing at a rate of 0.1 MPa/s until failure occurs. Strain gages are installed at the mid-section on top and bottom of the specimen surfaces.

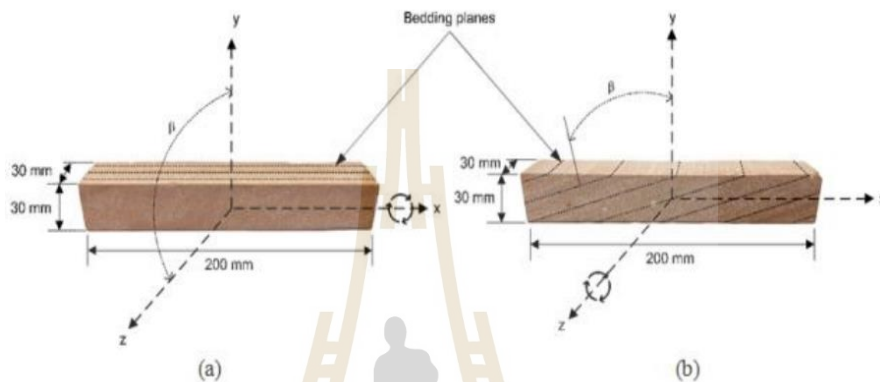


Fig. 1 Bedding plane orientations of Phu Phan sandstone specimens: (a) bedding plane strike parallel to x axis, and (b) bedding plane strike parallel to z-axis.

They are parallel and perpendicular to the main axis to measure compressive and tensile strains, as shown in Fig. 2. The strains are recorded with a data logger (TC-32K) connected to a switching box. Compressive and tensile stresses for four-point bending test induced at the top and bottom surfaces can be calculated by [12]:

$$\sigma_c = +PL/bd^2 \quad (1)$$

$$\sigma_t = -PL/bd^2 \quad (2)$$

where σ_c is compressive stress, σ_t is tensile stress, P is applied load, L is span length, b is specimen width, and d is specimen thickness.

IV. TEST RESULTS

Fig. 3 shows the induced tensile stress as a function of compressive and tensile strains under various bedding plane orientations for both cases. The maximum bending tensile strengths ($\sigma_{t,t}$) are found at $\beta = 0^\circ$ (bedding plane normal to loading direction) and lowest at $\beta = 90^\circ$ (bedding plane parallel to loading direction). For all the bedding plane orientations the tensile strength from case 1 is larger

than that from case 2, as shown in Fig. 4. The diagram in Fig. 4 also shows that the tensile strengths for both cases decrease as the angle β increases, where case 1 tends to give higher strength than case 2. For $\beta = 0^\circ$, both cases show identical results. Compressive (E_c) and tensile elastic moduli (E_t) can be calculated from the tangent at a linear portion of stress-strain curve (about 40-50% of failure stress).

The results are shown in Fig. 5 and Table 1. For case 2 the tensile elastic moduli (E_t) and the compressive elastic moduli (E_c) are largest when bedding planes are normal to loading direction ($\beta = 0^\circ$). For case 1 both tensile and compressive elastic moduli are greatest at $\beta = 90^\circ$. They gradually decrease to the lowest values at $\beta = 0^\circ$. The elastic moduli under tension for case 1 are greater than those for case 2. Fig. 6 shows that the Poisson's ratio increases under compression (ν_c) and tension (ν_t) as the bedding planes are rotated toward loading direction around z-axis. For both cases the tensile elastic moduli (E_t) are lower than the compressive modulus (E_c), and the Poisson's ratio under tension (ν_t) is slightly lower than that under compression (ν_c).

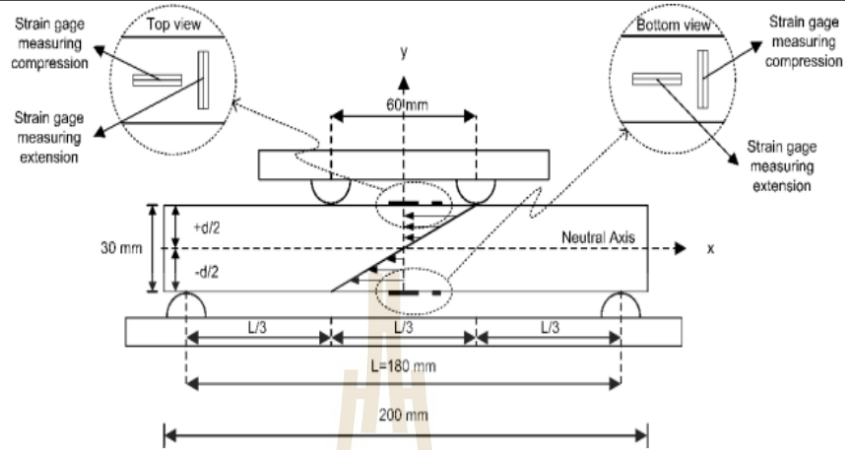


Fig. 2 Schematic diagram for four-point bending test with strain gage installation showing compressive and tensile stresses across the thickness of specimen.

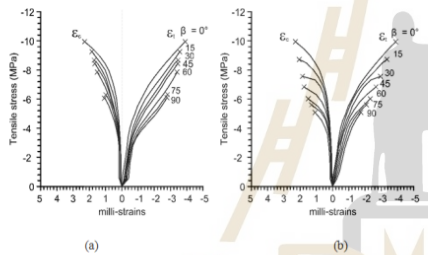


Fig. 3 Stress-strain curves with various bedding plane angles of case 1 (a) and case 2 (b).

intrinsic elastic parameters for bedding angle β of 0° and 90° . The intrinsic elastic parameters from the test results are shown in Table 2. The theory for Amadei's solutions has been described by many researchers [1],[10]-[11], [13]-[15]. Based on generalized Hook's law, Young's modulus and Poisson's ratio of transverse isotropic material can be calculated as:

$$E_y = 1/a_{22} \quad (3)$$

$$\nu_{yz} = a_{23}/a_{22} \quad (4)$$

where E_y is apparent Young's modulus in x, y and z coordinate systems, ν_{yz} is Poisson's ratio on y-z plane, and a_{22} and a_{23} are compliance components:

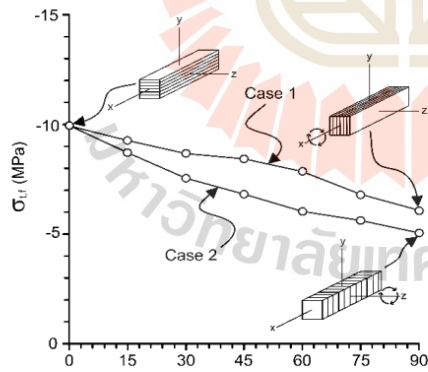


Fig. 4 Bending tensile strength as a function of angle β for both cases

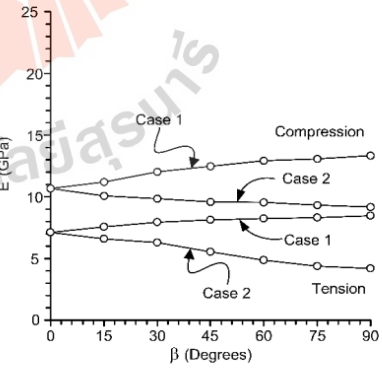


Fig. 5 Compressive and tensile elastic moduli as a function of angle β for both cases.

V. AMADEI'S SOLUTION

The obtained results are analyzed to determine the apparent elastic moduli under transverse isotropic effect. Amadei (1996) [1] presents the theoretical prediction for deformability of anisotropic rocks. The required test results for the calculation are the

$$a_{22} = \cos^4\beta/E' + \sin^4\beta/E + \sin^2 2\beta/4(1/G' - 2\nu'/E') \quad (5)$$

$$a_{23} = (\nu'/E')\cos 2\beta - (\nu/E)\sin^2\beta \quad (6)$$

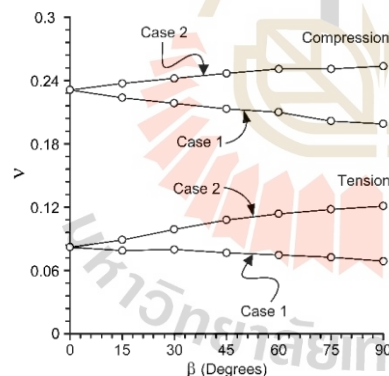
Effect of Transverse Isotropy on Tensile Strength and Elastic properties of Phu Phan Sandstone by Four-point Bending Test

where E and E' are the intrinsic Young's moduli on the transverse isotropy plane and in a direction normal to it, respectively, ν and ν' are the intrinsic Poisson's ratios characterizing the lateral strain response in the transverse isotropy plane parallel and normal to loading direction, G' is the shear modulus in planes normal to the transverse isotropy plane, and G is the shear modulus on transverse isotropic plane equal to $E/(2(1+\nu))$.

Fig.7 shows polar plots comparing the apparent elastic moduli (data points) with Amadei's predicted lines under different bedding plane angles. The apparent tensile elastic moduli under transverse isotropic effect show an elliptical shape, showing transverse isotropic effects under both compression and tension. The apparent compressive elastic moduli for the two cases are higher than those under tension.

Case	b (degrees)	σ_{1f} (MPa)	E_c (GPa)	E_t (GPa)	ν_c	ν_t
Case 1	0	9.94	10.68	7.10	0.23	0.08
	15	9.26	11.19	7.56	0.22	0.08
	30	8.67	12.02	7.93	0.22	0.08
	45	8.43	12.47	8.13	0.21	0.08
	60	7.85	12.92	8.24	0.21	0.07
	75	6.81	13.06	8.31	0.20	0.07
	90	6.08	13.32	8.47	0.20	0.07
Case 2	0	9.94	10.68	7.10	0.23	0.08
	15	8.72	10.07	6.58	0.24	0.09
	30	7.55	9.84	6.27	0.24	0.10
	45	6.83	9.60	5.53	0.25	0.11
	60	6.03	9.53	4.86	0.25	0.11
	75	5.62	9.33	4.38	0.25	0.12
	90	5.07	9.18	4.17	0.25	0.12

Table i. Tensile Strength and Elastic Parameters from four-point Bending Test Results.

Fig. 6 Poisson's ratios under compression and tension as a function of angle β .

The maximum apparent elastic moduli are found at bedding plane normal to loading direction in case 1. The apparent Poisson's ratios under compression and tension are shown in Fig. 8. The Poisson's ratios under tensile stress are less than half of those measured under compressive stress. Both cases show similar Poisson's ratio values. The bedding plane angle (β) has small effect on the Poisson's values.

The mean misfit can be used to evaluate the discrepancy between the test results and Amadei's prediction. The mean misfit (s_i) is calculated by [16]:

$$s_i = [(1/n) (\sum_{j=1}^n (X_{j,p} - X_{j,i})^2)]^{1/2} \quad (7)$$

where $X_{j,p}$ and $X_{j,i}$ are the predicted and measured apparent elastic moduli or Poisson's ratios, n is the number of bedding plane angles (β). The mean misfit for apparent compressive and tensile elastic moduli are 0.50, 0.32 GPa (for case 1), and 0.35, and 0.21 GPa (for case 2). For the apparent Poisson's ratios under compression and tension are 0.02, 0.02 (for case 1), and 0.01, and 0.05 (for case 2). The low values of mean misfit suggest that the Amadei's predictions agree well with the test results.

The degree of anisotropy of rock is determined by the maximum and minimum intrinsic elastic moduli ratio. The maximum and minimum elastic moduli can be measured normal and parallel to bedding plane orientation. Table 3 shows degree of anisotropy for both cases. Amadei et al. [1] suggest that the degree of anisotropy is normally in the range of 1 to 4, where each degree indicates quality of anisotropic rock such as low (1-2), intermediate (2-3) and high anisotropy (3-4). The results obtained from this study indicate that the degrees of anisotropy in terms of elastic

moduli under compression and tension for both cases are low, ranging from 1 to 2.

VI. DISCUSSIONS AND CONCLUSION

This study is to determine the effect of transverse isotropic plane on tensile strength and elastic properties of bedded sandstone by four-point bending test. The results obtained here tend to be similar to those of the three-point bending test, Brazilian test, direct tension test, and indirect tension test results obtained from other researchers [3]-[7]. Bending tensile strength for case 1 is higher than case 2 due to that the bedding plane is parallel to loading direction, which give low bending tensile strength. This agrees well with the four-point flexural results from Pires et al. [8]. Both elastic moduli and Poisson's ratios under tension are lower than those under compression. This is because the effort required to dilate the pore spaces and fissures in the rock is lower under tension than under compression. In general, the results obtained here agree reasonably well with those obtained by Fuenkajorn and Klanphumeesri [9]. The comparison between Amadei's prediction and test results of apparent elastic moduli and Poisson's ratios show

that the test data agree reasonably well with Amadei's predictions. The results from this study can be summarized as follows.

- Bending tensile strength is highest when bedding planes are normal to loading direction.
- The lowest tensile strength of the sandstone occurs when bedding plane strike is parallel to loading direction and having angle β equal to 90° .
- The elastic moduli and Poisson's ratios under tension are lower than those in compression. The tensile elastic moduli are about 65.18% and 56.64% of compressive elastic moduli for cases 1 and 2, respectively.
- For both conditions, bedding planes parallel to loading direction in z axis give lowest elastic moduli and gradually increases to greatest values when bedding planes are rotated to x axis at $\beta = 90^\circ$. Poisson's ratios under both conditions seem to be insensitive to the bedding plane angle.
- The degree of anisotropy of the sandstone used in this study is in the range of 1.16 - 1.70, which is classified as low anisotropy.

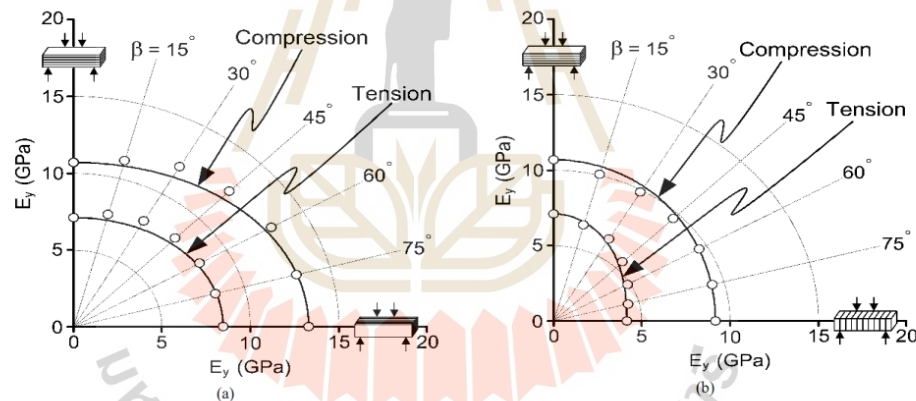


Fig. 7 Polar plots of apparent compressive and tensile elastic moduli for case 1 (a) and case 2 (b)

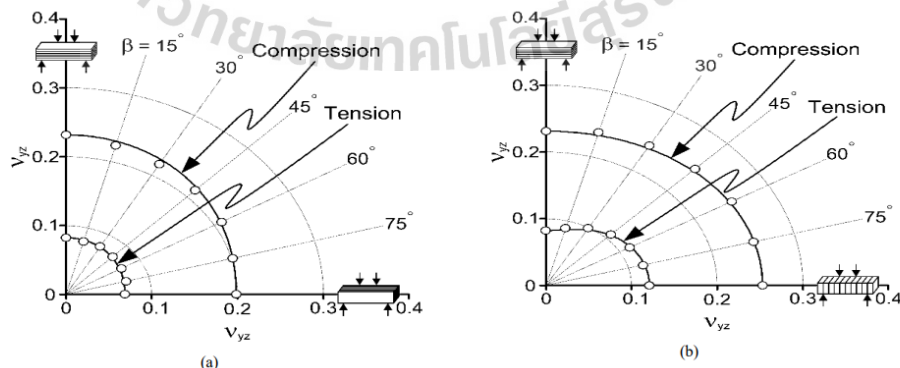


Fig. 8 Polar plots of apparent Poisson's ratios under compression and tension for case 1 (a) and case 2 (b)

Effect of Transverse Isotropy on Tensile Strength and Elastic properties of Phu Phan Sandstone by Four-point Bending Test

Case	Type of stress	E	E'	ν	ν'	G	G'
Case 1	Compression	13.32	10.68	0.20	0.23	5.48	4.46
	Tension	8.47	7.10	0.07	0.08	3.94	3.32
Case 2	Compression	9.18	10.68	0.25	0.23	3.70	4.26
	Tension	4.17	7.10	0.14	0.08	1.88	3.11

Table II. Intrinsic elastic Parameters Calculated from test Results for Amadei's Solution.

Case	Type of stress	E_{max}	E_{min}	Degree of anisotropy
Case 1	Compression	13.32	10.68	1.25
	Tension	8.47	7.10	1.19
Case 2	Compression	10.68	9.18	1.16
	Tension	7.10	4.17	1.70

Table III. Degree of anisotropy of phuphans and stone

ACKNOWLEDGEMENT

This work was supported by Suranaree University of Technology (SUT) and Thailand Science Research and Innovation (TSRI). Permission to publish this paper is gratefully acknowledged.

REFERENCES

- [1] B. Amadei, "Importance of anisotropy when estimating and measuring in situ stresses in rock," In International journal of rock mechanics and mining sciences & geomechanics abstracts, vol. 33, no. 3, pp. 293-325, Pergamon, 1996.
- [2] J. Plangklang, K. Arkhonghan, P. Tepnarong, and K. Fuenkajorn, "Time-dependent tensile strength of maha sarakham salt," Engineering Journal of Research and Development, vol. 28, no. 4, pp. 5-12, 2017.
- [3] F. Dou, J. G. Wang, X. Zhang, and H. Wang, "Effect of joint parameters on fracturing behavior of shale in notched three-point bending test based on discrete element model," Engineering Fracture Mechanics, vol. 205, pp. 40-56, 2019.
- [4] Z. Aliabadian, G. F. Zhao, and A. R. Russell, "Crack development in transversely isotropic sandstone discs subjected to Brazilian tests observed using digital image correlation," International Journal of Rock Mechanics and Mining Sciences, vol. 119, pp. 211-221, 2019.
- [5] S. Suwankeeree, "Effect of transverse isotropy on tensile strength and deformability of sandstone," School of Geotechnolgy Institute of Engineering Suranaree University of Technology, 2021. University of Technology, 2021.
- [6] J. J. Liao, M. T. Yang, and H. Y. Hsieh, H. "Direct tensile behavior of a transversely isotropic rock," International Journal of Rock Mechanics and Mining Sciences, vol. 34, no. 5, pp. 837-849, 1997.
- [7] C. S. Chen, and S. C. Hsu, "Measurement of indirect tensile strength of anisotropic rocks by the ring test," Rock Mechanics and Rock Engineering, vol. 34, no. 4, pp. 293-321, 2001.
- [8] V. Pires, P. M. Amaral, L. G. Rosa, and R. S. Camposinhos, "Slate flexural and anchorage strength considerations in cladding design" Construction and Building Materials, vol. 25 no. 10, pp. 3966-3971, 2011.
- [9] K. Fuenkajorn, and S. Klanphumeesri, "Direct Tension Tests of Intact Rocks Using Compression-to-Tension Load Converter." Engineering Journal of Research and Development, vol. 21, no. 2, pp. 51-57, 2010.
- [10] T. Thongprapha, K. Tengpakwaen, J. J. K. Daemen, and K. Fuenkajorn, "Effect of confining pressures on transverse isotropy of Maha Sarakham salt." International Journal of Rock Mechanics and Mining Sciences, vol. 152, pp. 105077, 2022.
- [11] M. Hakala, H. Kuula, and J. A. Hudson, "Estimating the transversely isotropic elastic intact rock properties for in situ stress measurement data reduction: a case study of the Olkiluoto mica gneiss, Finland," International Journal of Rock Mechanics and Mining Sciences, vol. 44, no. 1, pp. 14-46, 2007.
- [12] ASTM D672-17, Standard test method for flexural properties of unreinforced and reinforced plastics and electrical insulating materials by four-point bending, Annual Book of ASTM Standards, American Society for Testing and Materials, West Conshohocken, PA, 2020.
- [13] C.S. Chen, E. Pan, and B. Amadei, "Determination strength of anisotropic Brazilian tests of deformability and tensile rock using," Int J Rock Mech Min Sci, vol. 35, no. 1, pp. 43-61, 1998.
- [14] L. Yun-si, Z. Xiao, and Y. Quan, "The five elastic parameters for the anisotropy of slate under the influence of different bedding orientations," Electron J Geotech Eng, vol. 17, pp. 3695-3707, 2012.
- [15] R. Gholami, and V. Rasouli, "Mechanical and elastic properties of transversely isotropic slate," Rock Mechanics and Rock Engineering, vol. 47, no. 5, pp. 1763-1773, 2014.
- [16] K. F. Riley, M. P. Hobson, and S. J. Bence, "Mathematical methods for physics and engineering," A Comprehensive Guide. [Quantum operators], pp. 648-712, 1998.

BIOGRAPHY

Mr. Sujinda jakkawachote was born on November 4, 1997 in Kalasin Province, Thailand. He received his Bachelor's Degree in Engineering (Geological Engineering) from Suranaree University of Technology in 2020. For his post-graduate, He continued to study with a Master's degree in Civil, Transportation and Geo-resources Engineering Program, Institute of Engineering, Suranaree University of Technology. During graduation, 2020-2023, he was a part time worker in position of laboratory assistant at Geomechanics research unit, Suranaree University of Technology.

